JOURNAL OF ENGINEERING RESEARCH & SCIENCES

JENRS

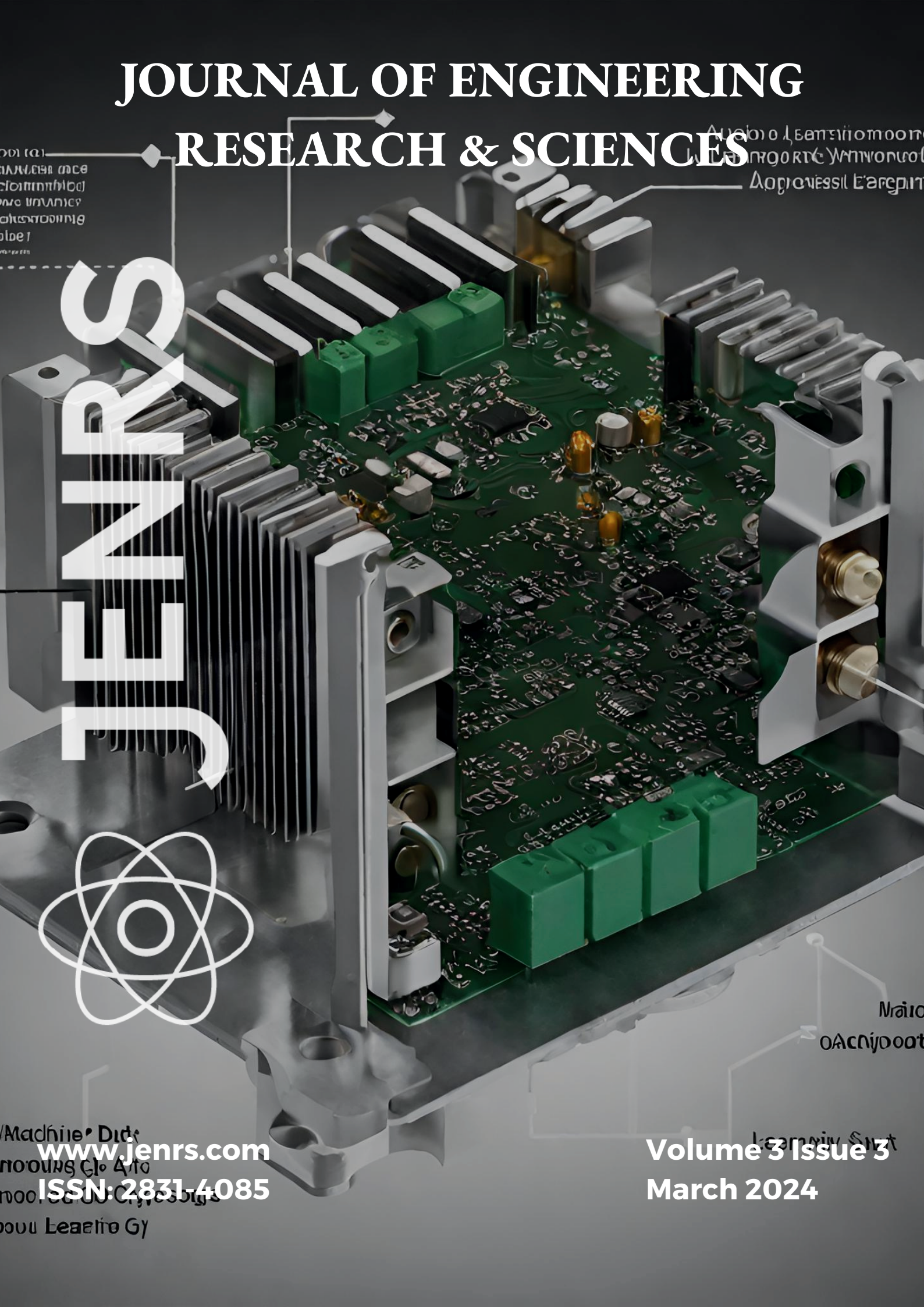

www.jenrs.com
ISSN: 2831-4085

Volume 3 Issue 3
March 2024

EDITORIAL BOARD

Editor-in-Chief

Editorial Board Members

Editorial

In this editorial, we present five papers that delve into critical issues spanning environmental responsibility, technological innovation, defence systems, and healthcare advancements. These papers contribute significantly to their respective domains, offering insights, solutions, and possibilities for future research and development.

As market economies advance, the pursuit of profits often overshadows environmental and social responsibilities, leading to the emergence of "greenwashing." This paper investigates the impact of Environmental, Social, and Governance (ESG) performance on Total Factor Productivity (TFP) in listed companies, particularly in China. Through empirical analysis, the paper demonstrates that higher ESG performance correlates with enhanced TFP, highlighting the importance of integrating sustainability practices into business strategies [1].

Field Programmable Gate Arrays (FPGAs) offer a versatile platform for real-time control algorithms, particularly in managing voltage spikes and static voltage errors in DC/DC boost converters. This paper explores the implementation of FPGA technology to mitigate voltage spikes, providing experimental evidence of its efficacy. By enabling dynamic control and parallel implementation of algorithms, FPGA technology presents a promising solution for addressing voltage irregularities in power systems [2].

Missile guidance systems play a pivotal role in ensuring tactical precision, with proportional navigation (PN) being a widely employed strategy. This paper introduces a comprehensive missile homing system incorporating true PN guidance, multiloop acceleration autopilot, and advanced imaging-based seekers. Leveraging deep machine learning for target detection and tracking, this system demonstrates superior performance in simulations, offering insights into the future of missile guidance technology [3].

Asthma remains a significant global health concern, affecting millions worldwide. This paper reviews recent advancements in intelligent monitoring systems, particularly those utilizing infrared sensors for asthma detection. By analyzing studies since 2016, the paper offers insights into evolving technologies and proposes a reference model for future research. These systems aim to enhance the quality of life for asthma patients by providing early detection and intervention strategies [4].

The papers presented in this editorial represent diverse areas of research, each addressing critical challenges and offering innovative solutions. From promoting sustainable business practices to advancing missile guidance technology and improving healthcare monitoring systems, these papers underscore the importance of interdisciplinary collaboration and technological innovation in addressing complex global issues. As we navigate an ever-changing landscape, the insights gleaned from these studies pave the way for future developments, fostering progress and resilience across various domains.

References:

[1] J. Zhang, Z. Liu, "'Greenwashing' or 'Helping': ESG Performance and Chinese Firm Total Factor Productivity," *Journal of Engineering Research and Sciences*, vol. 3, no. 3, pp. 1–12, 2024, doi:10.55708/js0303001.

[2] A. Barnawi, M. Zohday, "DC/DC Converter by using FPGA," *Journal of Engineering Research and Sciences*, vol. 3, no. 3, pp. 13–18, 2024, doi:10.55708/js0303002.

[3] M. Hodžić, N. Prljača, "Missile Guidance using Proportional Navigation and Machine Learning," *Journal of Engineering Research and Sciences*, vol. 3, no. 3, pp. 19–26, 2024, doi:10.55708/js0303003.

[4] A.Q. Al-Neami, Z.A. Abed, “Asthma Monitoring Systems Based on Electro-Infrared Sensors: A Review,” *Journal of Engineering Research and Sciences*, vol. 3, no. 3, pp. 27–32, 2024, doi:10.55708/js0303004.

Editor-in-chief

Prof. Paul Andrew

JOURNAL OF ENGINEERING RESEARCH AND SCIENCES

Volume 3 Issue 3 March 2024

CONTENTS

Received: 28 November, 2023, Revised: 20 February, 2024 Accepted: 21 February, 2024, Online: 19 March, 2024

DOI: https://doi.org/10.55708/js0303001

"Greenwashing" or "Helping": ESG Performance and Chinese Firm Total Factor Productivity

Jing Zhang, Ziyang Liu*

Graduate School, Kyonggi University, Suwon 16227, South Korea, zhangjing@kgu.ac.kr (J.Z.)

*Corresponding author: Ziyang Liu, Kyonggi University, Suwon Korea, victor@kgu.ac.kr

ABSTRACT: As the market economy has continued to develop, businesses have consistently prioritized profits, excessively emphasizing income and financial gains while neglecting ecological conservation and financial fraud. Consequently, the phenomenon of "greenwashing" has emerged. How to prevent this "greenwashing" phenomenon while pursuing economic benefits and enabling high-quality business development has become a focal point. Therefore, this paper analyzes whether the ESG (Environmental, Social, and Governance) performance of listed companies has an impact on the enhancement of the Total Factor Productivity (TFP) of enterprises. This study aims to explore how companies, while striving to maximize economic interests, can more proactively undertake environmental protection and social responsibility, thereby promoting the green transformation of enterprises. Using A-share listed companies from 2012 to 2022 as the sample, through an empirical examination of the correlation between the ESG performance of listed companies in China and the TFP of enterprises, the following conclusions are drawn: (1) ESG performance significantly promotes the TFP of enterprises, indicating that higher ESG performance corresponds to higher TFP; (2) Through intermediary effect tests, it is found that corporate reputation plays a role in enhancing the TFP of enterprises. That is, through good ESG performance, a company's reputation is improved, thereby leading to higher TFP; (3) Heterogeneity analysis demonstrates that the impact of good ESG performance on the enhancement of TFP is more significant in large-scale enterprises and state-owned enterprises.

KEYWORDS: ESG performance；Total Factor Productivity (TFP)；Corporate reputation

1. Introduction

Globally, issues concerning Corporate Social Responsibility (CSR) and Environmental, Social, and Governance (ESG) in sustainable development have garnered widespread attention. This attention originates not only from academia but also from governments, investors, media, and the general public. With shifts in policy orientation across the globe, more and more countries and regions are encouraging companies to fulfill their social and environmental responsibilities. ESG disclosure has become an integral part of a company's daily operations. For instance, the United Nations Sustainable Development Goals (SDGs) present a global consensus that demands active engagement from companies in addressing social and environmental issues. This is reflected in legislative and regulatory frameworks in numerous countries, offering policy support for corporate sustainability [1]. The proliferation of ESG disclosure is not merely a compliance requirement but has profound implications on business operations and investment decisions. Previous studies indicate that ESG disclosure aids in enhancing a company's reputation, reducing investment risks, and attracting more socially responsible investors [2]. This transformative shift is not confined to traditional CSR realms but encompasses operational performance closely associated with Total Factor Productivity (TFP). This paper's focal point is the relationship between ESG performance and TFP, with corporate reputation as the mediating variable. TFP is a crucial metric for assessing a company's performance, considering the comprehensive efficiency of multiple production factors[3,4]. The impact of ESG performance on TFP might be conveyed through various channels, with corporate reputation being a vital intermediary

mechanism. However, current research on how ESG performance affects TFP remains limited, especially in exploring mediating mechanisms [5]. This study aims to bridge this knowledge gap by delving into how ESG performance influences TFP through corporate reputation, providing practical guidance for corporate decision-makers, investors, and policymakers.

In recent years, more studies have started to focus on the relationship between ESG performance and TFP. In [6], the authors found a positive correlation between high ESG performance and higher TFP. They suggested that enhancing ESG performance might reduce environmental and social risks, enhance corporate reputation, and consequently affect TFP. Similarly, the research findings of [7] also indicate that companies with strong ESG performance exhibit higher TFP. However, these studies, while providing evidence, have certain limitations. Primarily, existing research often leans towards qualitative analysis or employs small samples, lacking large-scale quantitative analysis. This might limit the universality and robustness of the conclusions. Moreover, although some studies suggest that ESG performance may influence TFP through reputation channels, in-depth research into related mediating mechanisms remains relatively limited [8].

The innovative aspects of this study design will encompass several areas. Firstly, we aim to conduct comprehensive quantitative analysis using a large-scale dataset to address the deficiencies in current research [9]. This will contribute to a more comprehensive understanding of the relationship between ESG performance and TFP. Secondly, we will extensively investigate how ESG performance influences TFP through corporate reputation, exploring the details and pathways of the mediating mechanism. Finally, we will employ various methods, including robustness checks and heterogeneity analysis, to validate the robustness and universality of the research results, thereby enhancing the credibility of the study [10]. In summary, this paper aims to fill the research gap regarding the relationship between ESG performance and TFP, explore its mechanisms, and offer practical guidance for corporate decision-making and policy formulation. Through this research, we anticipate better comprehension of the connection between ESG and corporate operational performance, providing further insights for sustainable economic development.

2. Literature Review and Research Hypotheses

2.1. ESG Performance and Total Factor Productivity

According to the theory of information asymmetry, investors often require a substantial amount of relevant information to make decisions. In situations of severe information asymmetry, investors might make erroneous decisions, thereby reducing the allocation efficiency of the capital market. This leads to high-quality companies finding it challenging to obtain substantial funding for innovative activities, while less efficient companies can continue to acquire funds for less efficient production models. In [11], the authors demonstrated that the ESG rating of listed companies can reflect a company's level of corporate governance and effectively indicate the quality of information disclosure. There exists a significant positive correlation between these two aspects. Additionally, higher levels of corporate governance can effectively reduce situations where management sacrifices the company's long-term interests for personal gains due to agency problems and significantly curb the interests' encroachment by major shareholders [11–13]. By fully disclosing relevant information, companies enable investors to better understand their developmental status, facilitating the movement of capital in the capital market toward high-quality companies. Consequently, this enhances the ESG rating of listed companies, enabling companies to obtain more substantial resources for production activities, thereby increasing the total factor productivity of enterprises [14].

From a stakeholder theory perspective, if a company demonstrates excellent ESG performance, it can gain the trust of various stakeholders, thereby fostering the improvement of relationships among groups of stakeholders such as shareholders, employees, consumers, creditors, and the media. This leads to additional funding sources for external investments and internal research and development. Firstly, internal research and development, as a driving force for technological progress, enables companies to increase their knowledge reserves, optimize the combination of production factors, improve and upgrade production technology to enhance production efficiency. Additionally, research and development can help companies achieve technological innovation, providing new impetus for company development. Secondly, regarding external investments, limited resources can be invested in more efficient projects, thereby reducing the risk of resource misallocation and increasing total factor productivity [15]. Based on this, the following hypothesis is proposed:

H1: ESG performance contributes to enhancing the total factor productivity of enterprises.

2.2. ESG Performance, Corporate Reputation, and Total Factor Productivity

In the 1970s, signal transmission theory, stemming from information asymmetry theory, became a focal point for many scholars. Signal transmission theory is employed to alleviate information asymmetry. It posits that companies should timely disclose relevant internal information to enable outsiders to better understand the

company's actual operational status, thereby reducing information asymmetry. Moreover, to acquire external resources more effectively, internal personnel actively disclose information about the company to convey the company's operational situation to the external environment. Companies often use signals such as profits and incentives as financial indicators, while in the current scenario, ESG reports, non-financial indicator disclosures, have become an aspect that investors particularly focus on. Therefore, actively engaging in ESG disclosure essentially informs the market that the company considers the interests of various stakeholders during its operations, maintaining a positive stakeholder relationship, thus enabling the acquisition of more external resources [16–18].

Compared to companies that do not undertake social responsibility, socially responsible companies can transmit positive information about their good operational management to the outside world, thereby gaining the trust of more stakeholder groups, aiding the establishment of higher social reputation for the company [19]. Furthermore, corporate reputation is an intangible asset that allows companies to obtain capital from the outside, thereby alleviating the financing constraints of the company. Simultaneously, it increases the probability of attracting high-quality talents, which are crucial elements for company growth and also ensure the investment in human resources [19,20].

Hence, the following hypothesis is formulated:

H2: Corporate reputation acts as a mediator in the impact of ESG performance on the total factor productivity of enterprises.

3. Research Methods

3.1. Sample Selection

This study primarily investigates the impact of ESG performance of A-share listed companies on the total factor productivity of enterprises. Data were collected and organized through the Guotai An (CSMAR) database and the Wind Information (WIND) database. Using the Huazheng ESG rating data, the study period was set from 2012 to 2022, considering the availability of other key research variables. The data selection followed these criteria: (1) ST and *ST companies were removed; (2) companies from the financial and insurance industries were excluded; (3) samples with missing values were eliminated, resulting in an observed sample of 5993. To mitigate the influence of outliers on empirical results, a 1% winsorization was applied to continuous variables.

3.2. Variable Definitions

Dependent Variable: The total factor productivity (TFP) of enterprises was measured using methods such as OP, LP, OLS, etc. The study used the [21] and [22] methods to measure TFP through the LP method.

Explanatory Variable: The explanatory variable in this study is ESG performance. The study constructed the Huazheng ESG rating index by referencing mainstream ESG rating systems both domestically and internationally. Each indicator's applicability was deliberated to exclude unsuitable or unattainable data. Based on the rating criteria, ESG ratings were divided into 8 levels, from low to high: C, CC, CCC, B, BB, BBB, A, AA, and these ratings were used as the explanatory variable to measure a company's ESG performance.

Mediating Variable: After consulting relevant literature on corporate reputation, various foreign methods for measuring corporate reputation were examined, such as the "Most Admired Companies in America," "Global Most Admired Companies," and "Reputation Index" published by Fortune magazine. However, due to differences in cultural aspects between the East and the West, these methods might not be suitable for research on Chinese companies. Hence, building upon the work in [23], this study measured corporate reputation using intangible asset data.

Control Variables: Existing data suggests that factors such as company size, financial status, debt-paying ability, profitability, and corporate governance all impact the improvement of total factor productivity. Hence, referring to the methods of reference [24], the following control variables were selected: (1) Company Size (Size), (2) Company Age (Age), (3) Debt-to-Asset Ratio (Lev), (4) Return on Assets (ROA), (5) Fixed Asset Ratio (Fixed), (6) Company Growth (Growth), (7) Company Market Value (TobinQ), (8) Management Shareholding Ratio (Mshare), (9) Equity Concentration (Top10), and (10) Independent Director Ratio (Outdir). Definitions for related variables are detailed in Table 1.

3.3. Model design

To examine the impact of ESG performance on total factor productivity and explore the relationship between ESG performance, corporate reputation, and total factor productivity, a fixed-effects model based on the mediation effect testing method proposed [25] is established. To test the impact of ESG performance on overall factor productivity, the following model is designed:

$$TFP_{it}=\alpha_0+\alpha_1 ESG_{it}+\sum\alpha_j Controls_{it} + u_i + \lambda_t + \varepsilon_{it} \quad (1)$$

1. This model aims to investigate how ESG performance affects total factor productivity by considering various control variables.
2. Using corporate reputation as the dependent variable, the model aims to investigate the influence of ESG

performance on corporate reputation. The model is represented as:

$$Rep_{it} = \beta_0 + \beta_1 ESG_{it} + \sum \beta_j Controls_{it} + u_i + \lambda_t + \varepsilon_{it} \quad (2)$$

This model examines the impact of ESG performance on corporate reputation, incorporating control variables.

3. Incorporating both ESG performance and corporate reputation, this model examines whether corporate reputation mediates the relationship between ESG and total factor productivity:

$$TFP_{it} = \gamma_0 + \gamma_1 ESG_{it} + \gamma_2 Rep_{it} + \sum \gamma_j Controls_{it} + u_i + \lambda_t + \varepsilon_{it} \quad (3)$$

This model investigates the potential mediation effect of corporate reputation in the relationship between ESG and total factor productivity.

Here, I represents the enterprise, t represents the year, **Controls represents** the control variables, u_i represents individual fixed effects, λ_t **represents time fixed effects, and** ε_{it} represents the random disturbance term.

Table 1. Variable definition explanations

Variable type	Variable Names:	variable symbol	variable definition
Dependent Variable	High-Quality Development of Enterprises	*TFP*	Measurement of Total Factor Productivity using the LP method
Independent Variable	Enterprise ESG Performance	*ESG*	Assignment of values from 1-8 based on the Huazheng ESG rating from low to high
Mediating Variable	Corporate Reputation	*Rep*	Natural logarithm of Intangible Asset Net Value
Control Variable	Company Size	*Size*	Natural logarithm of Total Assets of the enterprise
	Company Age	*Age*	Age of the enterprise from its establishment to the specific period
	Asset-Liability Ratio	*LEV*	Total Liabilities to Total Assets ratio of the enterprise
	Asset Yield/Asset Profitability Ratio	*ROA*	Net Profit to Total Assets ratio
	Fixed Asset Ratio	*Fixed*	Net Fixed Assets to Total Assets ratio
	Company Growth Potential	*Growth*	Growth in Total Assets of the enterprise
	Company Market Value	*TobinQ*	Market Value to Total Assets ratio
	Management Holding Percentage	*Mshare*	Quantity of Management-held Shares to Total Shares
	Equity Concentration	*Top*10	Sum of the shareholding proportion of the top 10 shareholders of the enterprise
	Proportion of Independent Directors	*Outdir*	Proportion of Independent Directors among the total number of Board Members

Table 2: Descriptive statistics of variables

Variable name	Sample size	Mean value	Standard deviation	Minimum value	Maximum value
TFP	5993	8.634	1.115	4.706	13
ESG1	5993	3.965	1.162	1	8
Size	5993	22.608	1.313	18.524	28.293
Lev	5993	0.493	0.207	0.01	1.957
ROA	5993	0.03	0.075	-0.894	0.517
Cashflow	5993	0.047	0.078	-0.556	0.661
FIXED	5993	0.225	0.177	0	0.929
Growth	5993	0.276	2.175	-0.985	87.484
Indep	5993	0.374	0.059	0.167	0.714
Top10	5993	0.534	0.152	0.106	0.952
TobinQ	5993	2.025	2.16	0.674	76.82
Age	5993	3.058	0.244	1.946	3.761
Mshare	5993	0.036	0.111	0	1.694
Rep	5993	18.935	1.877	7.458	24.398

4. Analysis of empirical results

4.1. Descriptive Statistics

Descriptive statistical analysis, as depicted in Table 2, provides an overview of the collected data. This study gathered a total of 5993 valid samples, encompassing 14 variables. Among these variables, the total factor productivity (TFP) ranges from a minimum of 4.706 to a maximum of 13, with a standard deviation of 1.115. These values indicate significant differences in development across various industries in China.

The ESG performance (ESG1) of companies varies substantially, ranging from a minimum of 1 to a maximum of 8, with an average value of 3.965 and a standard deviation of 1.162. This highlights the considerable diversity in ESG performance among different companies.

Regarding corporate reputation (Rep), the average value is 18.935 with a standard deviation of 1.877. These figures illustrate significant differences in reputation among different enterprises. Such variability among the samples enhances the effectiveness of the empirical model analysis. The differences between samples enable more comprehensive matching in regression analysis, resulting in more credible and robust outcomes.

4.2. Correlation Analysis

The correlation analysis reveals significant relationships among the variables. From Table 3, it is evident that the correlation coefficient between ESG and total factor productivity is 0.276. This indicates a substantial positive association between ESG performance and total factor productivity, and the research findings are statistically significant at the 1% level. This result provides initial support for hypothesis H1, suggesting that ESG performance significantly enhances total factor productivity.

Furthermore, the analysis shows a strong correlation between corporate reputation and ESG performance, with a correlation coefficient of 0.153. Additionally, the correlation coefficient between corporate reputation and total factor productivity stands at 0.361, both achieving statistical significance at the 1% level. These results suggest that ESG performance elevates total factor productivity through the enhancement of corporate reputation, thereby providing preliminary validation for hypothesis H2.

Table 3: Correlation analysis of variables

Variables	TFP	ESG1	Size	Lev	ROA	Cashflow	FIXED	Growth	Indep	Top10	Tobin Q	Age	Mshare	Rep ut
(1) TFP	1.000													
(2)ESG1	0.276***	1.000												
(3) Size	0.737***	0.312***	1.000											
(4) Lev	0.361***	0.044***	0.415***	1.000										
(5) ROA	0.179***	0.189***	0.086***	0.357***	1.000									
(6)Cashflow	0.100***	0.047***	0.040***	0.205***	0.405***	1.000								
(7) FIXED	0.197***	0.050***	-0.004	-0.017	0.041***	0.232***	1.000							
(8) Growth	0.038***	0.041***	0.010	0.014	0.070***	0.006	-0.026*	1.000						
(9) Indep	0.016	0.096***	0.038***	0.000	-0.036**	0.040***	-0.034**	0.004	1.000					
(10) Top10	0.273***	0.084***	0.333***	0.083***	0.133***	0.085***	0.031**	0.048***	-0.036**	1.000				
(11)Tobin Q	0.301***	0.122***	0.391***	0.209***	0.013	0.018	0.074***	-0.011	0.029**	0.124***	1.000			
(12) Age	0.101***	0.095***	0.130***	0.060***	0.089***	-0.045***	-0.126***	0.023	0.040***	-0.019	0.026*	1.000		
(13) Mshare	-0.022	-0.008	0.088***	0.139***	0.099***	0.059***	-0.121***	0.053***	-0.003	0.006	0.007	-0.176***	1.000	
(14) Rep	0.361***	0.153***	0.560***	0.105***	0.075***	0.116***	0.220***	-0.026*	0.005	0.153***	-0.212***	-0.004	-0.027*	1.000

*** p<0.01, ** p<0.05, * p<0.1

Table 4: Variance Inflation Factor (VIF) Test

Variables	VIF	1/VIF
Size	1.78	0.561
Lev	1.54	0.65
ROA	1.32	0.759
ESG1	1.22	0.82
Age	1.17	0.855
Top10	1.15	0.87
TobinQ	1.1	0.909
Mshare	1.07	0.933
FIXED	1.05	0.949
Indep	1.02	0.982
Growth	1.00	0.998

In order to accurately mitigate the interference of multicollinearity among the variables, a VIF test was conducted. The analysis results, as presented in Table 4, reveal that all variables have VIF values less than 5. This indicates that there is no evidence of multicollinearity among the variables. Hence, the selection of variables is reasonable, and the analytical data results possess a higher level of reliability.

4.3. Hausman Test

Prior to conducting regression analysis, a Hausman test was employed to determine whether a fixed effects model or a random effects model should be selected. The test results, as displayed in Table 5, indicate that the test statistics for each variable are less than 0.01. This signifies that for this research, a fixed effects model is more suitable compared to a random effects model.

4.4. Baseline Regression Analysis

Following the research approach, a baseline regression was conducted to explore the relationship between a company's ESG performance and Total Factor Productivity (TFP). The results of the model are presented in Table 6. Model (1) includes Total Factor Productivity (TFP) and Company ESG1 performance alone, while Model (2) incorporates Total Factor Productivity (TFP), Company ESG1 performance, and control variables.

The analysis indicates that the value of ESG1 in Model (1) is 0.0454, and in Model (2), it stands at 0.0484. Both values are statistically significant at the 1% level, indicating a positive impact of a company's ESG performance on its Total Factor Productivity. In other words, as a company's ESG performance improves, its Total Factor Productivity tends to increase.

Table 5: Hausman Test

variable	(b)	(B)	(b-B)	sqrt(diag(V_b-V_B))
ESG1	0.008	0.011	-0.004	0.001
Size	0.525	0.562	-0.037	0.006
Lev	0.276	0.333	-0.057	0.014
ROA	1.46	1.548	-0.088	0.009
FIXED	-1.076	-1.018	-0.058	0.023
Growth	0.001	0.001	0.001	0.001
Indep	0.167	0.127	0.04	0.03
Top10	0.04	0.045	-0.005	0.023
TobinQ	0.004	0.004	0	0.001
Age	0.608	0.252	0.355	0.104
Mshare	0.351	0.281	0.07	0.032

b = Consistent under H0 and Ha; obtained from xtreg.

B = Inconsistent under Ha, efficient under H0; obtained from xtreg.

Test of H0: Difference in coefficients not systematic

chi2(5) = (b-B)'[(V_b-V_B)^(-1)](b-B) = 333.59

Prob > chi2 = 0.0000

Model (1) has an adjusted R-squared of 0.107, whereas Model (2), which includes control variables, exhibits an adjusted R-squared of 0.275. The higher adjusted R-squared in Model (2) compared to Model (1) suggests that the inclusion of control variables enhances the model's fit.

Table 6: Baseline Regression Results

	TFP	TFP
	(1)	(2)
ESG1	0.0454***	0.0484***
	(4.9122)	(6.3509)
Lev		1.0163***
		(18.1972)
ROA		2.1160***
		(20.5147)
FIXED		-1.2914***
		(-17.2327)
Growth		-0.0000
		(-0.9690)
Indep		0.0791
		(0.5050)
Top10		0.8605***
		(11.7103)
TobinQ		-0.0148***
		(-9.1943)
Age		1.2318***
		(36.8100)
Mshare		0.4258***
		(4.0982)
cons	8.3609***	3.9117***
	(225.0124)	(29.0693)
N	5993	5993
adj. R2	0.107	0.275

4.5. Mediation Analysis

The results of the mediation effect for company reputation are depicted in Table 7. Model (1) represents the regression model between the dependent variable and independent variable along with control variables in the absence of Reputation. Model (2) includes the regression model of the independent variable, control variables, and Reputation. Lastly, Model (3) displays the regression model between the dependent variable and independent variable after adding control variables and Reputation.

The regression outcomes reveal a significant impact of a company's ESG performance on the enhancement of Total Factor Productivity under the mediation effect of company reputation. Both Model (1) and Model (3) exhibit significant results for ESG performance at a 1% confidence level. Specifically, when a company's ESG1 performance increases by 1 unit, it leads to a 0.0471 unit increase in high-quality development for the enterprise. In Model (2), the mediator variable, company Reputation, shows a significant positive correlation with ESG ratings at a 1% level. This signifies the transmission role of company reputation between ESG ratings, indicating that an improvement in ESG performance enhances company reputation, further boosting Total Factor Productivity.

Table 7: Company Reputation Mediation Effect

	TFP	Rep	TFP
	(1)	(2)	(3)
ESG1	0.047***	0.070***	0.043***
	(6.07)	(4.05)	(5.50)
Rep			0.070***
			(10.12)
Lev	0.903***	0.667***	0.856***
	(14.16)	(4.75)	(13.55)
ROA	1.891***	0.067	1.887***
	(17.65)	(0.28)	(17.82)
FIXED	-1.027***	0.441**	-1.058***
	(-12.16)	(2.37)	(-12.67)
Growth	0.020***	0.004	0.020***
	(7.18)	(0.63)	(7.17)
Indep	0.175	-0.905**	0.239
	(1.05)	(-2.47)	(1.45)
Top10	0.849***	1.406***	0.750***
	(10.47)	(7.87)	(9.29)
TobinQ	-0.033***	-0.029***	-0.031***
	(-7.92)	(-3.18)	(-7.51)
Age	1.197***	-0.446	1.228***
	(5.64)	(-0.95)	(5.86)
Mshare	0.313***	1.023***	0.241**
	(2.79)	(4.14)	(2.17)
Y			0.070***
			(10.12)
cons	4.191***	18.230***	2.910***
	(6.50)	(12.83)	(4.48)
N	4783	4783	4783
R2	0.405	0.207	0.419
adj. R2	0.318	0.091	0.334

t statistics in parentheses

* $p < 0.1$, ** $p < 0.05$, *** $p < 0.01$

The resolution of images should not be less than 118 pixels/cm when width is set to 16 cm. Images must be scanned at 1200 dpi resolution and submitted in jpeg or tiff format. Graphs and diagrams must be drawn with a line weight between 0.5 and 1 point. Graphs and diagrams with a line weight of less than 0.5 point or more than 1 point are not accepted. Scanned or photocopied graphs and diagrams are not accepted.

4.6. Robustness Tests

4.6.1 Replacing the Dependent Variable

To test the robustness of the model, the dependent and independent variables were replaced. In the previous basic regression analysis, the ESG ratings from Huazheng were assigned numerical values according to their order. For robustness testing, following the methodology from previous research by [26] and [27], a reassignment of the Huazheng ESG ratings was done. Publicly available data indicate that these ratings can be categorized into three levels: A-rated companies are ESG performance leaders, B-rated companies represent average ESG performance, and C-rated companies lag behind. In this context, the ESG2 variable was assigned values according to these definitions to replace ESG1. Additionally, the alternative measurement methods for the dependent variable, Total Factor Productivity, were considered. Robustness testing included using the OP method, OLS method, and fixed-effect method to reevaluate Total Factor Productivity and use these new measurements as dependent variables.

In Table 8, Model (1) represents the replacement of the explanatory variable ESG1 with ESG2. Models (2), (3), and (4) represent the results of regressions using OLS, fixed-effect, and OP methods with different measurements of the dependent variable. The results show that ESG performance remains highly significant in all models at a 1% significance level. This consistency in results suggests that the model is robust.

4.6.2 Instrumental Variable

The baseline regression results indicate that the better the ESG performance, the stronger the positive effect on enhancing a company's total factor productivity. However, this result could also be due to the fact that companies with higher total factor productivity are more willing to actively improve their own ESG rating, potentially leading to a two-way causal endogeneity issue. To address this potential endogeneity issue, this paper employs lagged ESG performance and the industry average ESG performance as instrumental variables in a two-stage least squares regression. In the first-stage regression of the two-stage least squares method, the study uses the firm's ESG performance as the explained variable, the lagged ESG performance, and industry average ESG performance as explanatory variables, alongside the control variables From Model (1), controlling for industry and time effects in a least squares regression. In the second stage, the study employs the total factor productivity measured by the OP and LP methods as the explained variables and ESG performance as the explanatory variable for regression.

Table 8: Replacing the Dependent Variable

	TFP_LP (1)	TFP_OLS (2)	TFP_FE (3)	TFP_OP (4)
ESG1		0.0709***	0.0770***	0.0191***
		(8.4224)	(8.8641)	(2.6220)
ESG2	0.1248***			
	(7.0238)			
Lev	1.2301***	1.2503***	1.3103***	0.7495***
	(19.9518)	(20.2767)	(20.6031)	(14.0487)
ROA	2.3734***	2.3542***	2.4035***	1.9902***
	(20.8115)	(20.6719)	(20.4631)	(20.1982)
FIXED	-0.2301***	-0.2165***	-0.0589	-1.0492***
	(-2.7761)	(-2.6171)	(-0.6898)	(-14.6566)
Growth	-0.0001*	-0.0001*	-0.0001**	-0.0000
	(-1.8598)	(-1.9281)	(-2.0534)	(-0.7751)
Indep	-0.0789	-0.1321	-0.1822	0.2694*
	(-0.4559)	(-0.7635)	(-1.0210)	(1.8001)
Top10	1.2332***	1.2340***	1.3121***	0.6541***
	(15.1693)	(15.2100)	(15.6809)	(9.3184)
TobinQ	-0.0180***	-0.0182***	-0.0190***	-0.0123***
	(-10.1472)	(-10.2735)	(-10.3803)	(-8.0163)
Age	1.6894***	1.6823***	1.7672***	1.0993***
	(45.5806)	(45.5339)	(46.3758)	(34.3910)
Mshare	0.2287**	0.2391**	0.2112*	0.3907***
	(1.9898)	(2.0845)	(1.7849)	(3.9369)
cons	4.5909***	4.5490***	4.7424***	2.8117***
	(30.8029)	(30.6185)	(30.9489)	(21.8732)
N	5878	5878	5878	5878
adj. R^2	0.299	0.301	0.305	0.225

The regression results are presented in Table 9. It can be observed that in the first stage of Table 9, the regression coefficients of L.ESG and IndESG are both significantly greater than 0 at the 1% significance level. This indicates a high correlation between these two instrumental variables and the explanatory variables. The results of the weak instrumental variable test and over-identification test also demonstrate the effectiveness of the instrumental variable selection in this study. Looking at columns (2) and (3) of Table 9, the regression coefficients for ESG are 0.101 and 0.185, both significant at the 1% level. This demonstrates that, even after using instrumental variables to address potential endogeneity issues in the two-stage least squares regression, the conclusions of this study still hold, affirming that a strong ESG performance in companies can contribute to increased total factor productivity.

Table 9: Results of Instrumental Variable Regression

	First ESG (1)	Second TFP_OP (2)	Second TFP_LP (3)
ESG		0. 101***	0. 185***
		(17. 47)	(26. 61)
L. ESG	0. 774***		
	(145.65)		
IndESG	0. 066***		
	(3. 94)		
Control	YES	YES	YES
YEAR	YES	YES	YES
INDUSTRy	YES	YES	YES
_cons	0. 924***	5. 125***	6. 580***
	(7. 64)	(71.22)	(76.07)
N	5878	5878	5878
adj. R2	0. 614	0. 484	0. 552

4.6.3 Controlling for Individual Effects

To further address estimation biases caused by endogeneity, this study undertook regression analysis controlling for individual effects. Table 10 provides regression results simultaneously controlling for individual, industry, and yearly effects. From Table 10, it is observed that after controlling for individual effects, the coefficients for ESG are 0.0629, 0.0654, 0.1142, and 0.1194, all significant at the 1% level. This indicates that strong ESG performance in companies can enhance total factor productivity and affirms the prior research conclusion even after addressing potential endogeneity by controlling for individual effects.

4.6.4 Sample Selection Issue

This paper employs the Heckman two-stage regression to address potential sample selection issues. In the first stage Probit regression, the dependent variable DESG is a dummy variable. When ESG is greater than the mean, DESG is 1; when ESG is less than the mean, DESG is 0. The exogenous instrument variable remains the industry average of ESG performance (IndESG). The choice of the industry average of ESG performance as an exogenous instrument variable is because a company's ESG performance can be influenced by industry ESG performance, especially the industry environment, social responsibility awareness, and corporate governance, which can affect a company's ESG performance. Other control variables remain consistent with Model (1). The inverse Mill's ratio is calculated from the first-stage regression results, and it is included in the model for the second-stage regression. The regression results, as shown in the second column and third column of Table 11, demonstrate that the ESG regression coefficients for both OP and LP measures of total factor productivity are significant at the 1% level. This indicates that even after employing Heckman's two-stage regression to overcome potential sample selection issues, the study's conclusion remains valid, demonstrating the robustness of the research findings.

Table 10: Results of Regression Controlling for Individual Effects

variable	(1) TFP_OP	(2) TFP_OP	(3) TFP_LP	(4) TFP_LP
ESG	0. 0629***	0. 0654***	0. 1142***	0. 1194***
	(15. 22)	(16. 12)	(23. 60)	(24. 98)
Control	YES	YES	YES	YES
YEAR	NO	YES	NO	YES
INDUSTRY	NO	YES	NO	YES
FIRM	NO	YES	NO	YES
_cons	4. 8033***	4. 8910***	6. 4325***	6. 4697***
	(105. 99)	(80. 20)	(121. 30)	(90. 03)
N	5878	5878	5878	5878
Adj. R2	0. 4488	0. 5001	0. 5426	0. 5793
F	1713. 11	526. 8621	2495. 51	725. 0600

Table 11: Heckman Two-Stage Regression Results

variable DESG	(1) TFP_OP	(2) TFP_LP	(3)
ESG		0. 0796***	0. 1436***
		(19. 53)	(29. 47)
IndESG	0. 0935**		
	(2. 08)		
imr		1. 6762***	2. 1807***
		(10. 77)	(11. 72)
Control	YES	YES	YES
YEAR	YES	YES	YES
INDUSTRY	YES	YES	YES
_cons	0. 9302***	4. 6803***	6. 2011***
	(2. 76)	(71. 93)	(79. 72)
N	5787	5878	5878
Adj. R2		0. 4869	0. 5559
F		524. 3927	691. 3780

4.7. Further Research

4.7.1 Analysis Based on Scale Heterogeneity

Larger companies tend to hold leading positions within their industries due to their robust risk resilience and extensive funding sources, providing a secure foundation for the full realization of ESG's role. This subsequently aids companies in alleviating financing constraints and increasing research and development investments, thus enhancing total factor productivity. Accordingly, this study anticipates that the positive impact of excellent ESG performance on the total factor productivity of large-scale enterprises will be greater than that on small and medium-sized enterprises (SMEs). Therefore, In [28, 29], papers measures company size using the natural logarithm of total assets and groups the sample based on the mean of this indicator. Companies larger than the mean are categorized as large-scale enterprises, while those smaller than the mean are classified as SMEs. Subsequently, group regression and inter-group coefficient difference tests are conducted based on Model (1). Columns (1) and (2) in Table 12 provide the results of the group regression, showing that while the ESG coefficients in both sample groups are significantly positive, the regression coefficients in the large-scale enterprise sample (0.0744 and 0.1291) are higher than those in the SME sample (0.0095 and 0.0398). Moreover, the inter-group coefficient difference test also indicates significance at the 1% level, confirming the hypothesis that excellent ESG performance has a greater positive impact on the total factor productivity of large-scale enterprises compared to SMEs.

4.7.2 Heterogeneity Analysis Based on Property Rights

For state-owned enterprises, they possess stronger talent and technological advantages and tend to have easier access to funding sources during financing. Consequently, state-owned enterprises' research and development investments often enjoy more robust financial support, contributing to an improved total factor productivity. In this scenario, state-owned enterprises are better positioned to leverage the advantages of excellent ESG performance, translating it into impetus for increased research and development investments to enhance total factor productivity. Therefore, this study expects that excellent ESG performance has a greater positive impact on the total factor productivity of state-owned enterprises compared to non-state-owned enterprises.

Table 12: Heterogeneity Test Results Based on Scale

	(1)	(2)	(3)	(4)
variable	TFP_OP	TFP_OP	TFP_LP	TFP_LP
ESG	0. 0744***	0. 0095*	0. 1291***	0. 0398***
	(12. 95)	(1. 90)	(19. 83)	(7. 26)
Control	YES	YES	YES	YES
YEAR	YES	YES	YES	YES
INDUSTRY	YES	YES	YES	YES
_cons	5. 4618***	5. 6829***	7. 8087***	7. 4120***
	(51. 23)	(85. 13)	(64. 67)	(101. 60)
N	5787	5878	5787	5878
Adj. R2	0. 3843	0. 2829	0. 4481	0. 3346
F	150. 8827	121. 3907	195. 9741	154. 4751

Coefficient difference test between groups
Chi2(1) = 71. 15
Prob>Chi2 = 0. 0000
Chi2(1) = 106. 61
Prob>Chi2 = 0. 0000

To test the heterogeneous effects of ESG performance on the improvement of total factor productivity for state-owned and non-state-owned enterprises, this study uses a dummy variable based on the ownership nature. State-owned enterprises are represented as 1, while non-state-owned enterprises are represented as 0. Group regression is conducted based on Model (1), and inter-group coefficient difference tests are performed. Columns (3) and (4) in Table 13 present the regression results for the sub-samples of state-owned and non-state-owned enterprises.

The regression coefficients for ESG in state-owned enterprise results are 0.1072 and 0.1721, both significant at the 1% level. In the non-state-owned enterprise results, the ESG coefficients are 0.0527 and 0.1084, also significant at the 1% level. While both are significantly positive at the 1% level, the regression coefficient for state-owned enterprises is higher than that for non-state-owned

Table 13: Heterogeneity Test Results Based on Property Rights

variable	(1) TFP_OP	(2) TFP_OP	(3) TFP_LP	(4) TFP_LP
ESG	0. 1072***	0. 0527***	0. 1721***	0. 1084***
	(14. 51)	(10. 74)	(19. 56)	(18. 58)
Lev	1. 3074***	1. 4923***	1. 7763***	2. 2212***
	(23. 99)	(45. 49)	(27. 39)	(56. 92)
Control	YES	YES	YES	YES
YEAR	YES	YES	YES	YES
INDUSTRY	YES	YES	YES	YES
_cons	4. 8553***	5. 1079***	6. 6820***	6. 6744***
	(41. 67)	(68. 11)	(48. 18)	(74. 81)
N	4564	5878	4564	5878
Adj. R2	0. 5018	0. 4409	0. 5588	0. 5040
F	184. 4533	289. 8876	231. 6766	373. 3346

enterprises. Moreover, the inter-group coefficient difference test is significant at the 1% level, indicating that excellent ESG performance has a more substantial positive effect on the total factor productivity of state-owned enterprises compared to non-state-owned enterprises.

5. Conclusion and Enlightenment

5.1. Research Conclusions

This study focuses on A-share listed companies from 2012 to 2022, utilizing the Huazheng rating index to measure corporate ESG performance and validating the correlation between ESG performance and total factor productivity of listed companies. The main conclusions drawn from this research are as follows:

ESG Performance and Total Factor Productivity: ESG performance significantly enhances a company's total factor productivity. This implies that higher ESG performance correlates with increased total factor productivity.

Effect of Corporate Reputation: Empirical analysis demonstrates that a company's reputation significantly influences the enhancement of its total factor productivity. This indicates that improving a company's reputation through good ESG performance further elevates its total factor productivity. Furthermore, these conclusions remain robust after various sensitivity tests such as altering the computation method of the explained variable, alternative assignment methods for explanatory variables, implementing instrumental variable methods to alleviate potential endogeneity issues, and utilizing the Heckman two-stage method to correct sample selection biases.

Heterogeneity Analysis: The research shows that the impact of good ESG performance on enhancing total factor productivity is more pronounced in large-scale enterprises and state-owned enterprises.

5.2. Policy Insights

Based on the conclusions drawn in the previous sections, the paper proposes policy recommendations in the following areas:

Policy Formation: Governments should expedite the formulation of laws and regulations governing corporate ESG performance to establish a robust institutional framework, directing policies to steer companies toward high-quality development. This includes fostering environmentally friendly practices and preventing inadequate or untimely disclosures, thus discouraging unethical behaviors born from insufficient information, such as illegal waste disposal or opportunistic practices.

Enhanced Regulatory Oversight: Regulatory authorities should intensify their focus on corporate ESG performance by implementing stricter laws, establishing robust regulatory mechanisms, and employing more robust measures to maintain market order. Introducing third-party audit mechanisms for comprehensive assessment and evaluation of a company's ESG performance would ensure its quality and credibility.

Balanced Perspective on ESG Performance: Companies should adopt a balanced perspective on the unique role of ESG performance. They should invest efforts into achieving a win-win scenario in terms of economic and social benefits based on their specific circumstances. Acknowledging the necessity of improving ESG performance for sustainable development, companies can align economic and social benefits, promoting organizational legitimacy for their high-quality development.

This research provides practical policy implications to promote sustainable business practices and organizational growth.

Conflict of Interest

The authors declare no conflict of interest.

References

[1] X. Deng, W. Li, X. Ren. "More Sustainable, More Productive: Evidence from ESG Ratings and Total Factor Productivity among Listed Chinese Firms." Finance Research Letters, vol. 51, no. 3, pp. 789–795, 2023, doi.org/10.1016/j.frl.2022.103439.

[2] N. Li, X. Wang, Z. Wang, X. Luan. "The Impact of Digital Transformation on Corporate Total Factor Productivity." Frontiers in Psychology, vol. 13, no. 5, pp. 1544–1553, 2022, doi: 10.3389/fpsyg.2022.1071986.

[3] G. Ge, X. Xiao, Z. Li, Q. Dai. "Does ESG Performance Promote High-Quality Development of Enterprises in China? The Mediating Role of Innovation Input." Sustainability, vol. 14, no. 7, pp. 3843, 2022, doi.org/10.3390/su14073843.

[4] Q. Xia, Y. Liu, F. Wei. "How Can ESG Funds Improve Their Performance? Based on the DEA-Malmquist Productivity Index and fsQCA Method." zgkxjsdxxb, vol. 53, no. 4, pp. 0803–0809, 2023, doi：10.52396/justc-2023-0017.

[5] X. Su, S. Wang, F. Li. "The Impact of Digital Transformation on ESG Performance Based on the Mediating Effect of Dynamic Capabilities." Sustainability, vol. 15, no. 18, pp. 13506, 2023, doi.org/10.3390/su151813506.

[6] L. Sun, N.A.M. Saat. "How Does Intelligent Manufacturing Affect the ESG Performance of Manufacturing Firms? Evidence from China." Sustainability, vol. 15, no. 4, pp. 2898, 2023, doi: 10.3390/su15042898.

[7] G. Sun, C. Guo, J. Ye, C. Ji, N. Xu, H. Li. "How ESG Contribute to the High-Quality Development of State-Owned Enterprise in China: A Multi-Stage fsQCA Method." Sustainability, vol. 14, no. 23, pp. 15993, 2022, doi.org/10.3390/su142315993.

[8] F. Wang, Z. Sun. "Does the Environmental Regulation Intensity and ESG Performance Have a Substitution Effect on the Impact of Enterprise Green Innovation: Evidence from China." International Journal of Environmental Research and Public Health, vol. 19, no. 14, pp. 8558, 2022, doi.org/10.3390/ijerph19148558.

[9] Y. Shen, H. Zheng, H. Cai, X. Chen, Y. Liu, S. Ma, X. Zhao. "ESG Performance, R&D Innovation and High Quality Development of Corporate: A Perspective Based on Firm Performance." Industrial Engineering and Innovation Management, vol. 5, no. 6, pp. 23–34, 2022, https://www.nature.com/articles/s41565-019-0603-y.

[10] P. Yang, X. Hao, L. Wang, S. Zhang, L. Yang. "Moving toward Sustainable Development: The Influence of Digital Transformation on Corporate ESG Performance." Kybernetes, vol. 53, pp. 1544–1553, 2023, doi.org/10.1126/sciadv.1501122.

[11] R. Yao, Y. Fei, Z. Wang, X. Yao, S. Yang. "The Impact of China's ETS on Corporate Green Governance Based on the Perspective of Corporate ESG Performance." International Journal of Environmental Research and Public Health, vol. 20, no. 3, pp. 2292, 2023, doi.org/10.1002/ani.202116068.

[12] J. Zheng, Y. Jiang, Y. Cui, Y. Shen. "Green Bond Issuance and Corporate ESG Performance: Steps toward Green and Low-Carbon Development." Research in International Business and Finance, vol. 66, pp. 102007, 2023,doi.org/10.1016/j.ribaf.2023.102007 .

[13] Y.P. Chen (Vincent), Z. Zhuo, Z. Huang, W. Li. "Environmental Regulation and ESG of SMEs in China: Porter Hypothesis Re-Tested." Science of The Total Environment, vol. 850, pp. 157967, 2022, doi.org/10.1016/j.scitotenv.2022.157967.

[14] D. Zhang, L. Liu. "Does ESG Performance Enhance Financial Flexibility? Evidence from China." Sustainability, vol. 14, no. 18, pp. 11324, 2022, doi.org/10.3390/su141811324.

[15] D. Zhang. "Does Green Finance Really Inhibit Extreme Hypocritical ESG Risk? A Greenwashing Perspective Exploration." Energy Economics, vol. 121, pp. 106688, 2023, doi.org/10.1016/j.eneco.2023.106688 .

[16] D. Zhang, L. Meng, J. Zhang. "Environmental Subsidy Disruption, Skill Premiums and ESG Performance." International Review of Financial Analysis, vol. 90, pp. 102862, 2023, doi.org/10.1016/j.irfa.2023.102862.

[17] P. Moskovics, P. Wanke, Y. Tan, A.M. Gerged. "Market Structure, ESG Performance, and Corporate Efficiency: Insights from Brazilian Publicly Traded Companies." Business Strategy and the Environment, doi:10.1002/bse.3492.

[18] S. Li, E. Xie. "The Effect of Economic Growth Target Constraints on ESG." Applied Economics Letters, vol. 0, pp. 1–4, 2023, doi: 10.1002/bse.3492.

[19] A. Babkin, E. Shkarupeta, L. Tashenova, E. Malevskaia-Malevich, T. Shchegoleva. "Framework for Assessing the Sustainability of ESG Performance in Industrial Cluster Ecosystems in a Circular Economy." Journal of Open Innovation: Technology, Market, and Complexity, vol. 9, pp. 100071, 2023, doi: 10.1016/j.joitmc.2023.100071.

[20] C. Li, S. Ba, K. Ma, Y. Xu, W. Huang, N. Huang. "ESG Rating Events, Financial Investment Behavior and Corporate Innovation." Economic Analysis and Policy, vol. 77, pp. 372–387, 2023, doi.org/10.1016/j.eap.2022.11.013.

[21] Y. Luo, Z. Lu, C. Wu, C.N. Mensah. "Environmental Regulation Effect on Green Total Factor Productivity: Mediating Role of Foreign Direct Investment Quantity and Quality." International Journal of Environmental Research and Public Health, vol. 20, no. 4, pp. 3150, 2023, doi.org/10.3390/ijerph20043150, .

[22] L. Chen, M.U. Khurram, M.Z. Abedin, yuyang Gao, B.M. Lucey. "ESG Disclosure and Technological Innovation Capabilities of the Chinese Listed Companies." 2022, doi.org/10.1016/j.ribaf.2023.101974.

[23] W. Ma, Y. Li, L. Ding. "Does Marine Financial Policy Affect Total Factor Productivity of Marine Enterprises? An Empirical Evidence Based on Chinese First Guidance on Strengthening Finance for Marine Economy." Marine Pollution Bulletin, vol. 195, pp. 115493, 2023, doi.org/10.1016/j.marpolbul.2023.115493.

Jing Zhang got master's degree from Kyonggi University, and currently a doctoral student. He is producer of China Education Television, and my research direction is ESG and brand management. I have published several related papers so far.

Ziyang Liu received the PhD in management from the Kyonggi University and am currently an assistant professor at the University, specializing in brand management and sustainability.

Received: 16 September, 2023, Revised: 13 February, 2024, Accepted: 26 February, 2024, Online: 19 March, 2024
DOI: https://dx.doi.org/10.55708/js0303002

DC/DC Converter by using FPGA

Amin Barnawi*, Mohammed Zohday
Department of Engineering and Computer Science, Oakland University, Rochester, 48309, USA
*Corresponding author: Amin Barnawi, email: barnawi@oakland.edu

ABSTRACT: This paper discusses FPGA technology and assesses how this technology can be implemented to eliminate voltage spikes. This study also evaluates how FPGA can be used to remove the static voltage errors from the DC/DC boost converter. This technology is used to remove the voltage spikes when the impedance load is changed instantly. The FPGA stands for field programmable gate array. This system is used to control the dynamic behavior of a such system in practice. Through the use of this FPGA technology, it is very easy to implement such control algorithms that can able to work in real-time, and also their sampling period is very low. The required output can be achieved through the parallel implementation of control algorithms. In this paper, there are some experimental results through the use of FPGA technology in boost converter.

KEYWORDS FPGA, boost converter, dynamic behavior of voltages, DC/DC converter, switching converter.

1. Introduction

1.1. Background

The use of DC/DC converters in the field of electricals features prominently in applications such as the power supplies used in electronic circuits. The DC/DC converter is also used in DC electric motors and for converting high-level and low-level DC voltages. The load impedance can be changed using different capacitance and inductive loads. The condition in which the voltage overshooting occurs at the output of the DC-DC converters so this condition is not reliable for these converters and may cause damage to the other electrical appliances like the electric motor. Later on, whenever the sudden change in the output voltage occurs, this change occurs when the loading impedance changes. This is quite real whenever any voltage disturbance occurs in any electrical appliances due to voltage overshoot, so this FPGA technology covers that phase of voltage overshoot in any electrical system.

1.2. Conceptual Clarification

For the practical measurement, some experiments have been performed by making a model of a DC-DC boost converter and using FPGA technology. The model can be implemented through different impedances in the circuit. In MATLAB, different simulations have been proposed regarding this boost converter. In this report, some experiments have been proposed by using this concept.

2. Literature Review

According to the author Spino, he has proposed a work about the DC/DC boost converter this has to be done through the use of FPGA technology. A correct model for the DC/DC boost converter has been presented through FPGA technology implementation. The two hardware designs of the converter have been presented through different FPGA footprints. This explicit design of the buck-boost DC/DC converter has been designed and this design will help to allow efficient circuit implementation. In this paper, two controllers have been implemented on FPGA [1].

For the DC-DC converter, how feed-forward controller can be implemented? The conventional DC/DC converter topologies like buck, boost, Cuk and buck-boost converters have their controlling techniques for certain applications. The voltage regulator is used to maintain the constant voltages at the output of these converters whenever a current or voltage change occurs at the input of these converters. For this, a range of control techniques has been implemented for linear and nonlinear control of these converters. These controlling techniques are used to overcome the dynamic changes in the output of the system. These controllers can be classified as proportional, proportional-integral-dynamic, and also proportional-integral. These all controllers are used to control the active behavior of these converters. This linear control of the converter is not sufficient to face high changes in the line voltages and also in load current. But the nonlinear control techniques like the Fuzzy logic control, genetic algorithm, Adaptive Neutral Network, and also many other controlling techniques are used to increase the performance of these converters. Many controlling techniques have been implemented through the use of FPGA technology.

For controlling the output voltage of these converters PID auto-tuning technique is used. This technique is used to control the DC/DC boost converters through the use of relay feedback techniques. The controller parameters are used to maintain the output level of these converters.

These parameters of the controllers are used to control the output of these converters. This controller parameter is tuned and used as the PID regulator. This technique is used to remove the effect of parasitic resistance and inductance in the output capacitor of these converters. That produces a lot of noise at the output of the DC/DC converter so by using this technique of feedback control through the PID controller this noise can be reduced easily.

The author Elshaer has proposed a control technique for the DC-DC boost converter that is a PID controller in a Photovoltaic system. This controller can be tuned with the help of a Genetic algorithm for the regulation of the output voltage. For tuning the proportional, integral, and derivative gain of this PID controller the Fuzzy-PID controller was used. For controlling the duty cycle of the boost converter, a smart controller was used in this research. For the fixed frequency at the input, a nonlinear controller was proposed. For the power amplifier, a four-switch non-inverting Buck-boost converter is used that is based on the sliding mode control strategy. The ideal advantage of using this controller is that this controller will help to increase the performance, efficiency, and energy of the system using these converters [2].

According to the author Fumio, he has designed a nonlinear controller called the fuzzy controller, and this controller is used to regulate a Cuk converter and also the boost converter. A complete study has been carried out for the output of these converters [3]. According to the author Gupta, he has proposed a fuzzy logic controller for controlling the output of the bulk and boost converters for a common algorithm of this converter. For the experimental implementation of this controller, an 8-bit microcontroller is used. This Fuzzy logic controller is used for the steady-state output of the boost converter [4].

Mattavelli describes the aim of the Fuzzy controller for the bulk-boost converter. In this research, the simulation results have been proposed and also proposed a control methodology. According to the author Raviraj, he has developed a linear PI controller, fuzzy controller, and also the sliding mode controller [5].

In this paper, the author Tseng has proposed a high-performance design for the DC/DC switching power converter like the Boost converter. This converter is involved in providing a regulated voltage of 50 and a current of up to 15 amperes. For getting a high range of adjustable voltage at the output of the converter a PI gain control scheme has been designed through the use of an FPGA chip. In this paper experimental results also have been proposed. Through the use of FPGA technology, the issue of limited adjustable output voltage range for these PWM switching converters has been resolved. Also, this technique increases the efficiency of the output of the system. Using the ZVS technique, the output efficiency of the system improved [6].

According to the author Hyo-Sik, he has proposed a fuzzy controller for the boost and buck converter. And this can be done using a digital signal possessor whose processor is switched at 10 MHz frequency. Then after that, an integrated Fuzzy controller is designed and used for the boost converter control and this can be done through the current mode control technique [7].

3. Mathematical Model of the System

3.1. DC/DC boost converter

The DC/DC converter is shown in the figure 1.

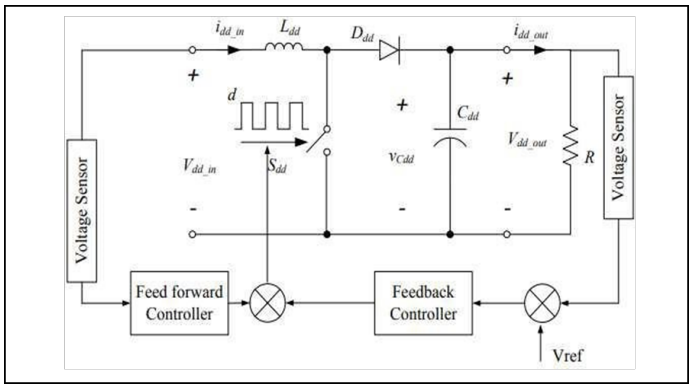

Figure 1: DC/DC Boost Converter

3.2. Parameters of the DC/DC Boost Converter

For the parameter first of all there is a demonstration of the specifications of the DC/DC boost converter. The input voltage of the converter is set to 400 volts. The inductor, capacitor, and load resistor values are calculated through their formulas. The inductor value is 2.9×10^{-3}. For the setting of IGBT FET resistance is 0.1 and put the snubber capacitance at infinity. For the setting of the diode of the boost converter, the resistance is set at 0.001, the snubber resistance is set at 500, and the snubber capacitance is at 250×10^{9}. The capacitor for the boost converter is set at 1×10^{-6} the value of the load resistor is set at 20 ohms and the value of the boost converter is not according to the requirement that has been set in the problem. Based on these specifications, the parameters for the DC/DC boost converter have been calculated.

The switching frequency of this power-rated boost converter is set to 5 kHz. For finding the inductance value, in the first step find the resistances value according to the diagram and then calculate the value of the duty cycle ratio. After this find the rated input current of the inductor. Then through the input current ripple, the value of the inductor used for this boost converter can be found easily. The capacitor value of this boost converter can be calculated through the output voltage ripple ratio. The peak switch voltage is equal to the input voltage for this boost converter. The current value of this power diode is 150 A. The phase change in the circuit is measured by the IBC circuit design using MATLAB/Simulink software.

3.3. Design of Feed Forward Control

The DC/DC boost converter is very important in the field of electrical like the electric motors are controlled through these converters. The feed-forward controller has been designed for the DC/DC boost converter. This feedback controller has been designed by measuring open loop line regulations that are for the fixed load and can be set up to 5 percent and the DC input voltage can be changed by 400%.

After using this converter, the load regulation was also good without the use of a negative feedback loop.

The feed-forward control of this converter consists of a comparator. The voltage divider for this controller is composed of two resistors that are R1 and R2 and the comparator for this controller is an operational amplifier that is supplied by only a single voltage source V. The v_t is the sawtooth and this voltage is applied at the non-inverting input of the comparator. The peak value of the Sawtooth of voltage is denoted by V_{TM} and this value is set up to 5-10 voltages. The switching frequency of this converter is set according to the frequency of the saw tooth voltage. For the input of this comparator, the reference voltage is applied as the inverting input of the comparator. And this reference voltage is denoted by V_{REF}. This reference voltage can be written as

$$VREF \quad \frac{R2}{R1 \;\; R2} * V1 \;\; \alpha V1 \tag{1}$$

In the equation the α $\frac{R2}{R1R2}$ the output of this comparator is like a rectangular wave and this wave is used as the gate to source the voltage of the MOSFET. For increasing the output current of the rectangular wave and this wave is used as the gate to source the voltage of the MOSFET. For increasing the output current of the comparator, for this, attach the non-inverting buffer between the power MOSFET and the comparator [8]. For this, the on-duty cycle of the power transistor can be defined as

$$D \quad \frac{t_{on}}{T} \tag{2}$$

In this equation, the t_{on} is the period when this power MOSFET is on and the period of this is equal to $T \;\; 1t$

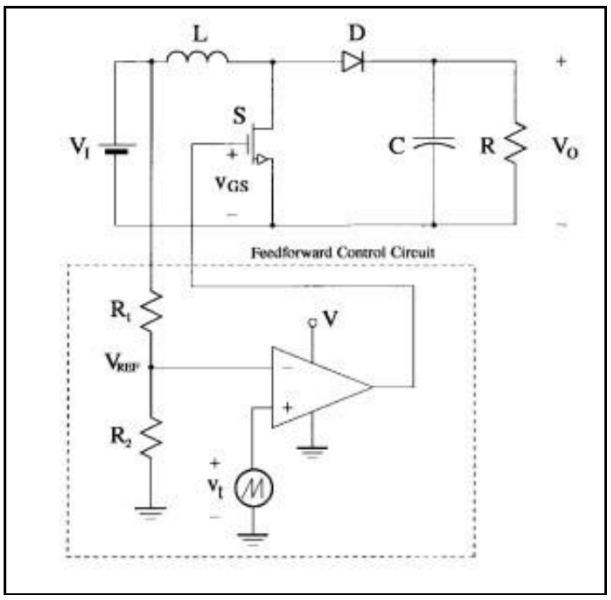

Figure 2: Schematic of the prototype

The prototype of the system that will be implemented using MATLAB Simulink [9] is shown in figure 2 The IBC system development is based on the desired objectives and produced an output voltage that is approximately equal to the desired voltage. The conventional boost converter indicates higher efficiency, high reliability, low ripple current, and lower voltage ripples.

$$\frac{VTM}{T} \quad VREF\,[(1-D)\,T]\,(1-D)\,T \tag{3}$$

$$V1\,[(1-D)\,T]\,(1-D)\,T * \frac{R2}{R1 \;\; R2} \tag{4}$$

After arranging these values this can be written as

$$D \quad \frac{VREF\,(1-D)\,T}{VTM} \tag{5}$$

$$\frac{\alpha * V1\,(1-D)\,T}{VTM} \tag{6}$$

The output voltage of this feed-forward controller can be found as

$$V_o \quad \frac{1}{1-D} * V1 \tag{7}$$

Through the substitution of the values, the output voltage can be written as

$$V_o \quad \frac{VTM}{\alpha} \tag{8}$$

$$V_o \quad \left(\frac{R1}{R2} \;\; 1\right) * VTM \tag{9}$$

The operational amplifier can be used as the comparator when its slew rate is high enough and the slew rate can be found by assuming the value of the rise time and fall time of the gate-to-source ratio. The slew rate of the operational amplifier can be calculated.

$$SR \quad \frac{\Delta V_{GS}}{tr} \tag{10}$$

$$SR \quad \frac{20\Delta V_{GS}}{T} \tag{11}$$

$$SR \quad 20fs\Delta V_{GS} \tag{12}$$

In this equation, the ΔV_{GS} is the peak-to-peak voltage from the gate to the source voltage [10].

For designing the control system for this boost converter set the voltage reference at 1 and for designing the PID controller set the proportional part of the PID controller at 0.7, the integral part of the PID controller is set at 100, and for the advanced setting of this controller. The upper saturation limit is set at 1 and the lower saturation limit at 0.1. Attached are the DC-DC PWM generator setting the switching frequency at 5000 and the sampling time up to 1×10^{-6}.

The operational amplifier can be used as the comparator when its slew rate is high enough and the slew rate can be found by assuming the value of the rise time and fall time of the gate-to-source ratio. The slew rate of the operational amplifier can be calculated.

4. Simulation Results

MATLAB/Simulink platform is used to perform the simulation of the DC-DC boost converter. The simulation results showed that the proposed converter configuration has higher energy productivity compared to traditional converter designs.

The design of the boost converter is implemented on MATLAB Simulink is shown in figure 3.

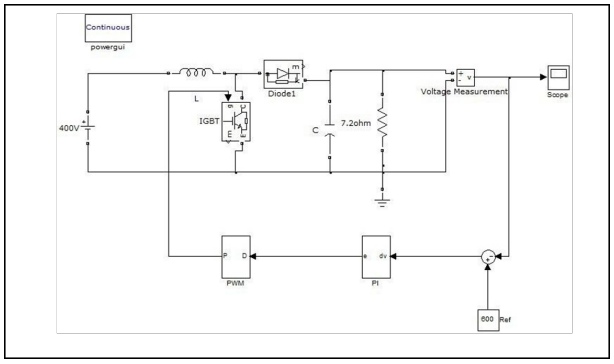

Figure 3: Design of boost converter

The voltage waveform of the boost converter can be seen through the help of the scope. The voltage is regulated by changing the duty cycle. Figure 4 shows the produced signal by using the waveform Editor (*.vwf). In the present situation, the time for on-off switching is considered to compare with the calculated values.

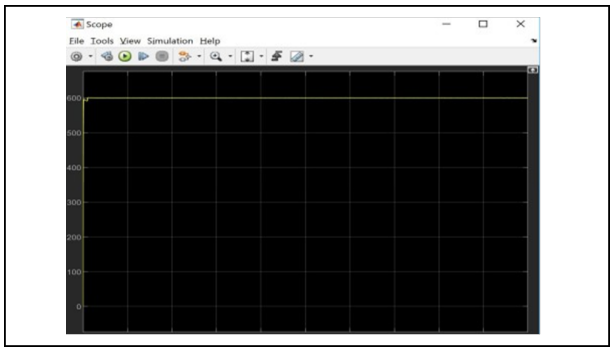

Figure 4: Waveform Editor

The inside of the feedback controller is like that by setting the gain value of 1/20 the design of the controller is like. The controller diagram is shown in the figure 5.

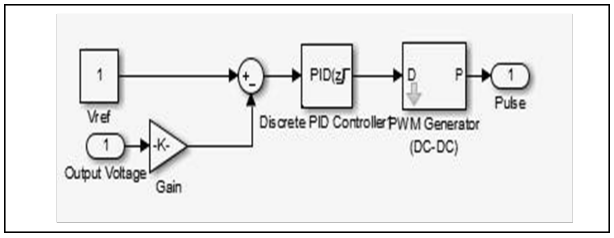

Figure 5: Controller

The system with the calculation of the transfer function was modeled in Simulink for control form as shown in Figure 6.

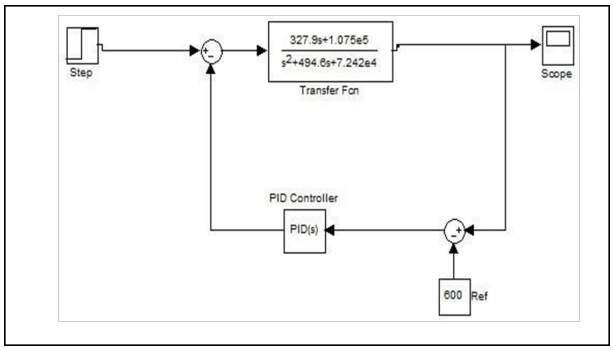

Figure 6: Simulink function

The voltage waveform after attaching the feed-forward controller the output voltage is also almost according to the requirement. The figure depicts output voltage that is slightly different from the calculated values. the control of the duty cycle on both sides of the whole phase is related to the change in voltage. The controllable output voltage is demonstrated is shown in figure 7.

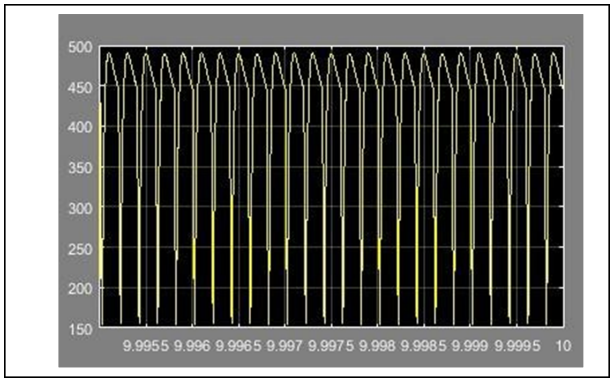

Figure 7: Voltage Output

5. Development of an FPGA-Based Controller Algorithm

A block diagram as shown if figure 8 shows the required process to develop the FPGA controller algorithm. It starts with writing Verilog code for the switching controller, which describes how the controller works it should meet the hardware requirements. After that, with good verification assign the I/O pins, because any mistake in this will affect the downloading of the code to the FPGA board. Finally, implement the hardware to verify that the controller code design successfully does its function.

Figure 8: Voltage Output

The relationship between the output voltage to the input voltage and duty cycle (D) is described in the following table.

Table 1: Relationship of output and input

Converter Equation	Output Voltage Style
Buck	Vout = Vin * D
Boost	Vout = Vin/(1-D)

6. Case Study Non-Inverting Buck-Boost Converter

Here we have chosen a Non-Inverting Buck-Boost converter as a case study to implement the FPGA control algorithm the figures 9 and 10 shows how the circuit looks like.

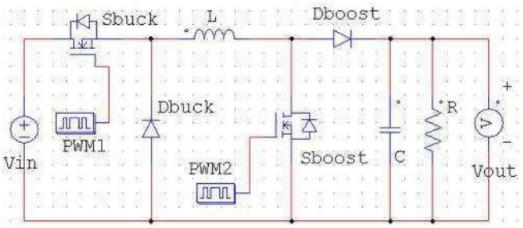

Figure 9: Circuit 1

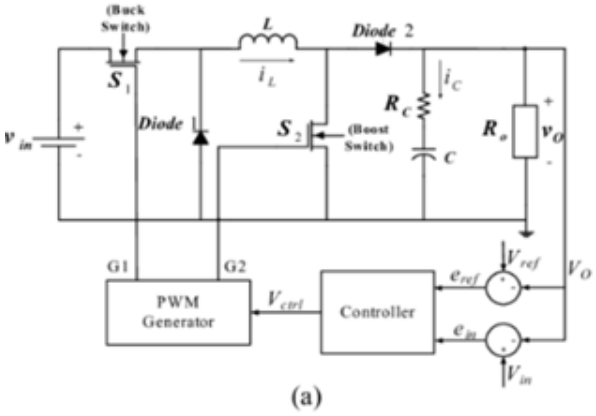

Figure 10: Circuit 2

So now from the table and the figure it is clear the relationship between V_{in}, V_{out}, and D (duty-cycle) is. It is also obvious from the equations in the previous sections we can start to make the flowchart of the control algorithm as shown in the figure 11.

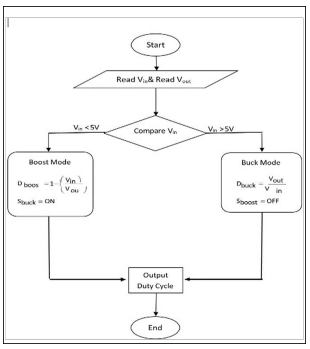

Figure 11: Flowchart showing FPGA controller algorithm development process in buck book converter

So now we got our flowchart which describes how the process flows to give us our control algorithm. The Verilog code of the voltage control loop is as follows.

module Voltage_control_loop (Vin, Vout, Dboost, Dbuck); input [2:0] Vin, Vout; output [4:0] Dboost, Dbuck; reg [4:0] Dboost, Dbuck; always @(Vin or Vout) begin
if (Vin < 5)
Dboost=1-(Vin/Vout);
else
Dbuck=Vout/Vin;
end module

6.1. Simulation of the Voltage Control Using Cadence Software

Starting to check if the algorithm we developed successfully controls the voltage as we want, we simulate our algorithm using cadence software as shown in figure 12.

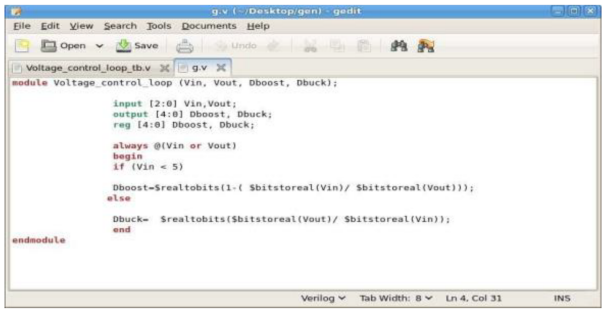

Figure 12: Veilog code

After writing the Verilog code in cadence and did run it, we got the following result as shown in figure 13.

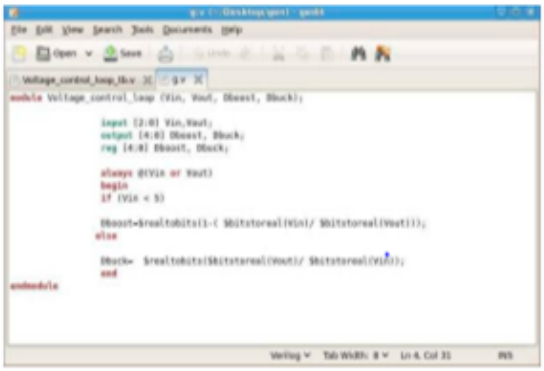

Figure 13: Veilog code in Cadence

7. Conclusion

It is concluded that boost converters are very valuable for electrical applications. For removing the ripples at the output of the boost converter a control technique can be implemented that is used to remove the voltage spikes from the output of the boost converter. In this report, a system is implemented for removing the line variation and the variation at the output of the boost converter can be done. For removing these errors at the output, a technique of feed-forward controller is used as the feedback of this boost

converter. For setting the value of the parameters of the boost converter a feedback controller can be designed. In this report, the parameters for the feed-forward are designed by setting the values of input voltages. For this report, it can be seen that the line voltages are quite better when the high load impedance is implemented. At the output of the load regulation, load regulation is perfect at the output of the boost converter. Also, in this report, we showed how to develop a control algorithm using FPGA technology. The algorithm was implemented and tested and it works well but it has to be tested in real hardware to verify its efficiency and figure out any issue to be solved.

References

[1] V. Spinu, A. Oliveri, M. Lazar, and M. Storace., "FPGA implementation of optimal and approximate model predictive control for a buck-boost DC-DC converter.," In Control Applications (CCA), 2012 IEEE International Conference on IEEE, pp. 1417- 1423, 2012, DOI: 10.1109/CCA.2012.6402444

[2] M. Elshaer, A. Mohamed and O. A. Mohammed., "Smart optimal control of DC-DC boost converter for intelligent PV systems," In Intelligent System Application to Power Systems (ISAP), 2011 16th International Conference IEEE, pp. 1-6, 2011, DOI: 10.1109/TDC-LA.2010.5762913

[3] T. I. I. O. a. M. S. F.Ueno, "Regulation of Cuk converters using fuzzy controllers," In Telecommunications Energy Conference, 1991. INTELEC'91., 13th International, IEEE, pp. 261-267, 1991.

[4] R. Gupta, R. G. Lamba, and M. I. G. Singh, "A Comparative Study of Conventional and Fuzzy Logic Control of DC Drive with Power Factor Correction," PhD diss, 2012.

[5] P. Mattavelli, L. Rossetto, G. Spiazzi and P. Tenti, "General-purpose fuzzy controller for DC-DC converters.," IEEE Transactions on Power Electronics, 1997, vol. 12, no. 1, pp. 79-86,

[6] K-H.Tseng and C.-L. Chen, "Design and hardware implementation for a full-bridge phase-shift PWM DC/DC converter system with FPGA-based PI gain-scheduling control.," In Industrial Electronics and Applications (ICIEA), 2011 6th IEEE Conference on, IEEE, pp. 1578-1582, 2011, DOI: 10.1109/ICIEA.2011.5975842

[7] H.-J. K. Hyo-Sik Park, "Simultaneous control of DC-DC converters by DSP controller," ICPE (ISPE), pp. 203-207, 2001.

[8] C. Yao, X. Ruan, W. Cao and P. Chen., "A two-mode control scheme with input voltage feed-forward for the two-switch buck-boostDC–DC converter.," EEE Transactions on Power Electronics, 2014 vol. 29, no. 4, pp. 2037-2048, DOI: 10.1109/TPEL.2013.2270014

[9] P. Karamanakos, T. Geyer and S. Manias., "Direct voltage control ofdc–dc boost converters using enumeration-based model predictive control," IEEE Transactions on Power Electronics, vol. 29, no. 2, pp. 968-978, 2014, DOI: 10.1109/TPEL.2013.2256370

[10] J. C. Rosas-Caro, J. M. Ramirez, F. Z. Peng and A. Valderrabano, "A DC-DC multilevel boost converter." IET Power Electronics, pp. 129-137, 2010, DOI: 10.1049/iet-pel.2008.0253

Received: 23 January, 2024, Revised: 29 February, 2024 Accepted: 11 March, 2024, Online: 19 March, 2024
DOI: https://dx.doi.org/10.55708/js0303003

Missile Guidance using Proportional Navigation and Machine Learning

Mirza Hodžić, Naser Prljača*
Control systems and Robotics, Faculty of electrical engineering, University of Tuzla, Tuzla, 75000, Bosnia and Herzegovina
*Corresponding author: Prljača Naser, Franjevačka 2 Tuzla 75000, naser.prljaca@fet.ba

ABSTRACT: Variants of proportional navigation (PN) are perhaps mostly used guidance laws for tactical homing missiles. PN aims to generate commanding missile lateral acceleration proportional to line of sight (LOS) angular rate, so that missile velocity vector rotates in such a way to assure interception of a target. In order to generate commanding lateral accelerations, the guidance system needs measurements of LOS angular rate and the closing velocity between the missile and the target, or the missile velocity. A device which provides guidance information is referred to as the missile seeker. In the case of imaging based seekers (visible light (EO), infrared light (IIR)), LOS rate is estimated using imaging sensor, while closing or missile velocity is measured using appropriate sensors or guess estimated. In this paper, we present the design and simulation of a missile homing system which includes: true PN guidance law, linear multiloop acceleration autopilot, and gimbaled imaging based missile seeker. Target seeker uses advanced deep machine learning object detection YOLO (You only look once) model, for target detection and tracking as well as LOS rate estimation. Comprehensive simulation model, consisting of full 6DOF missile and controls dynamics, 3D world and camera model, is developed. Intensive simulation results show performances of the proposed missile homing system.

KEYWORDS Missile guidance, YOLO, Missile seeker, Proportional navigation, 6DOF

1. Introduction

Many missile guidance and control laws have been developed in the past. Reported missile autopilot designs have ranged from classical linear to the most advanced ones [1]–[4]. The most widely used guidance law among them is a variant of proportional navigation(PN) [5]–[8]. Homing missiles using a variant of proportional navigation (PN) guidance law require measurement of LOS angular rate and measurement of closing velocity or missile velocity. This implies that missile seeker is able to detect and track targets during engagement. In active homing missiles, radar based missile seeker is used to detect the target, track the target and measure LOS rate and closing velocity. In passive homing missiles, strap-down or gimbaled imaging sensor (EO/IIR) based missile seeker is used to detect the target, track the target and estimate LOS angular rate, while missile velocity is measured with an appropriate sensor (IMU). In this work, a two axis (pitch and yaw) gimbal carrying an imaging device keeps the target in the camera field of view (FOV) by means of a gimbal control tracking loop. Accurate measurement of tracking error is of essential importance for tracking accuracy and LOS rate estimation. Tracking error is obtained by locating targets within the image using appropriate image processing techniques. Thanks to rapid advances in deep machine learning(convolutional neural networks), high accuracy and high speed deep learning object detection models have emerged. The most prominent among them is the YOLO (You only look once) family [9]. This work investigates application of YOLO deep machine learning object detector for tracking error measurements and consecutive LOS angular rate estimation in missile seeker. YOLO performance assessment in guidance loop is realized by means of a comprehensive Matlab/Simulink simulator, which includes nonlinear 6DOF missile and controls dynamics as well as 3D world (scene) and imaging models. This work was motivated by the fact, that to the best of the authors knowledge, no published work has been found which deals with similar simulation study.

2. Missile 6-DOF dynamic model

In order to simulate missile guidance, a high-fidelity nonlinear model is needed. Cruciform missile can be modeled as a rigid body which is governed by a system of coupled nonlinear first order differential equations with constant coefficients:

$$\dot{P} = L/I_x \tag{1}$$
$$\dot{Q} = PR\left(I_z - I_x\right)/I_y + M/I_y \tag{2}$$
$$\dot{R} = PQ\left(I_x - I_y\right)/I_z + N/I_z \tag{3}$$

$$\dot{u} = vR - wQ + F_x/m \tag{4}$$
$$\dot{v} = wp - uR + F_y/m \tag{5}$$
$$\dot{w} = uQ - vP + F_z/m \tag{6}$$

Where u, v and w are missile velocities along x, y and z axes of the missile body frame. P, Q and R are rotational angular velocities about x, y and z axes of the missile body frame. F_x, F_y and F_z are forces which are acting along the respected body axes and L, M and N are moments which are acting along the respected body axes. I_x, I_y and I_z are moments of inertia about the missile body axes. Inertia cross products are zero since the missile airframe is symmetric. For a cruciform missile, aerodynamic forces can be approximated as follows [10]:

$$\begin{bmatrix} F_x \\ F_y \\ F_z \end{bmatrix} = \begin{bmatrix} C_{x_0} + C_{x_2}\left(\alpha^2 + \beta^2\right) \\ C_N\beta \\ C_N\alpha \end{bmatrix} \tag{7}$$

Total force on acting along the missile body axes can:

$$\begin{bmatrix} F_x \\ F_y \\ F_z \end{bmatrix} = \begin{bmatrix} T \\ 0 \\ 0 \end{bmatrix} + mg \begin{bmatrix} -\sin\theta \\ \sin\phi\cos\theta \\ \cos\phi\cos\theta \end{bmatrix} - qS \begin{bmatrix} C_{x_0} + C_{x_2}\left(\alpha^2 + \beta^2\right) \\ C_N\beta \\ C_N\alpha \end{bmatrix} \tag{8}$$

Where $q = \rho v_m^2/2$ is the dynamic pressure, q is the density of air at given altitude and v_m is the total velocity of the missile. The gravitational force is naturally given in earth reference frame so it has to be transformed to body axes frame. In the previous equation, C_{x_0} and C_N are aerodynamic coefficients calculated at the various angles of attack α and sideslip angles β. Angle of attack and sideslip angle can be calculated as follows:

$$\alpha = \arctan\frac{w}{v} \tag{9}$$

$$\beta = \arctan\frac{v}{u} \tag{10}$$

Furthermore, it is important to define Euler RPY angles which describe the orientation of the missile with respect to the inertial reference frame. Euler angles can be integrated from the following equation:

$$\begin{bmatrix} \dot\phi \\ \dot\theta \\ \dot\psi \end{bmatrix} = \begin{bmatrix} 1 & \sin\phi\tan\theta & \cos\phi\tan\theta \\ 0 & \cos\phi & -\sin\phi \\ 0 & \frac{\sin\phi}{\cos\theta} & \frac{\cos\phi}{\cos\theta} \end{bmatrix} \begin{bmatrix} P \\ Q \\ R \end{bmatrix} \tag{11}$$

Moments acting on the missile are a consequence of rotation of actuator surfaces and of forces acting on the missile. Aerodynamic forces are acting on the point called the center of pressure, while the gravitational force is acting on the center of gravity of the missile. This causes a moment which rotates the missile. Therefore, the missile moments can be calculated as follows:

$$\begin{bmatrix} L \\ M \\ N \end{bmatrix} = \begin{bmatrix} 0 \\ -r_X F_{AZ} \\ r_X F_{AY} \end{bmatrix} + \frac{qS}{v_m} \begin{bmatrix} C_{LP}P \\ C_{MQ}Q \\ C_{NR}R \end{bmatrix} + qS \begin{bmatrix} C_{L\delta_E}\delta_E \\ C_{M\delta_V}\delta_V \\ C_{N\delta_P}\delta_P \end{bmatrix} \tag{12}$$

In the previous equation, r_x is the distance between center of gravity and center of pressure and F_{AY} and F_{AZ} are aerodynamic forces acting along the missile body axes. C_{LP}, C_{MQ} and C_{NR} are rolling, pitching and yawing aerodynamic coefficients respectively. $C_{L\delta_E}$, $C_{L\delta_V}$ and $C_{L\delta_P}$ are aerodynamic coefficients with respect to the angular displacement of actuator surfaces denoted by δ_E, δ_V and δ_P. Table 1 shows used missile parameters [11].

Table 1: Missile parameters

I_x	I_y, I_z	m	C_{x_2}
0.024 kgm^2	0.958 kgm^2	11.25 kg	0.484
C_{x_0}	$C_{N\delta_P}$	$C_{M\delta_V}$	$C_{L\delta_E}$
2.04	0.0905	0.0905	0.0905
C_N	C_{MQ}	C_{NR}	C_{LP}
3.298	−10	−10	0.0905
T	r_x	ρ	S
750 N	−0.119 m	1.225 kg/m^3	0.0314 m^2

3. Proportional navigation

The basic intuition of proportional navigation(PN) [12] is to generate commanding lateral accelerations which are proportional to the line of sight rate (LOS) angular rate as follows:

$$a_c = N\dot\lambda v_c \tag{13}$$

Where a_c is the commanded lateral acceleration normal to the line of sight, $N \geq 2$ is the effective navigational ratio and v_c is the relative velocity between the missile and the target. These commanded accelerations are then forwarded to the autopilot which makes sure that the missile achieves these lateral accelerations. In recent works, authors simulated this guidance method on 6-DOF missile simulator in Matlab in [13] and [14]. For even more insight into missile guidance and control, the reader is referred to [10], [11], [15]–[21]. As is shown in figure 1, in order to calculate λ or $\dot\lambda$ it is needed to measure relative distance and relative velocity between the missile and the target.

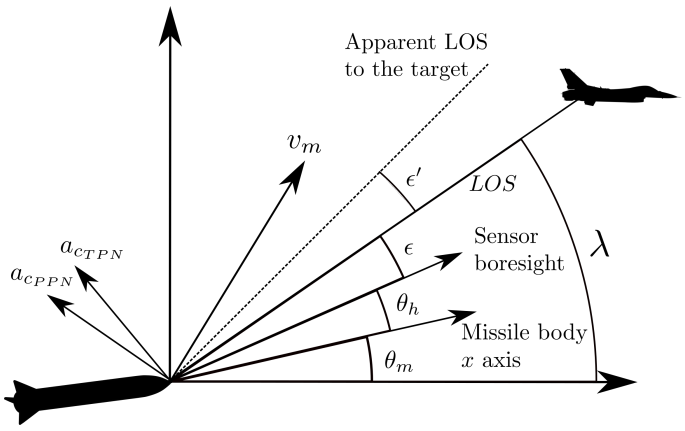

Figure 1: Geometry of proportional navigation

Unfortunately, these values cannot be measured without an active radar which most tactical missiles do not have. Similarly, the closing velocity v_c cannot be measured without an active radar. That is why this article implements another variant of PN called the pure proportional navigation whose commanding accelerations are normal to the missile velocity [12] and are given by:

$$a_c = N\dot\lambda v_m \tag{14}$$

Missile seeker is the device that has to measure LOS rate. The seeker is made out of two independent gimbal axes, two

servo motors and an imaging (EO/IIR) sensor. These two gimbals move across the vertical and the horizontal plane in order to lock onto the target. Once locked, the seeker can measure the tracking error, which is noted with ϵ in figure 1. Earlier work [14], [22]–[25] explain in great detail on how to obtain LOS and LOS rate from the measured tracking error. The LOS angular rate in vertical plane can be obtained using the following equation:

$$\dot{\lambda}_{z_m} = \epsilon_z \frac{s}{\tau s + 1} + \dot{\theta}_h + \dot{\theta}_m \tag{15}$$

Where θ_m is the Euler pitch angle of the missile relative to the inertial frame of reference, θ_h is the angular position of the gimbal servo relative to the missile centerline in vertical plane and ϵ_z is the measured tracking error in the vertical plane. Angular velocity $\dot{\theta}_m$ is easy to obtain using rate gyro as is explained in [14] and $\dot{\theta}_h$ has to be calculated from measured angular rates around the body axes as is explained in [13]. Similar to equation 15, LOS rate in the horizontal plane can be obtained as follows:

$$\dot{\lambda}_{y_m} = \epsilon_y \frac{s}{\tau s + 1} + \dot{\psi}_h + \dot{\psi}_m \tag{16}$$

Where ψ_m is the Euler yaw angle of the missile relative to the inertial frame of reference, ψ_h is the angular position of the gimbal servo relative to the missile centerline in the horizontal plane and ϵ_y is the measured tracking error in the horizontal plane. Most tactical missiles have infrared homing seeker. Because of this, tracking error cannot be measured directly but it is assumed to be indicated angular position of the target relative to the camera centerline or boresight [10]. This paper aims to simulate a seeker sensor which utilizes Matlab 3D camera, which would measure the tracking error from obtained images. Matlab interface for Unreal Engine allows simulations of 3D vehicles as well as taking images from Unreal Engine world. Also, implementation, simulation and control of gimbal servo system are presented in this article since it is guidance requirement to keep the tracking error as low as possible.

4. Autopilot design

If the missile lateral accelerations are exactly equal to the commanded accelerations commanded by the guidance subsystem, then the interception is guaranteed. Missile subsystem which will ensure this is referred to as the autopilot. From the missile dynamic model, it can be shown that there will be no cross-coupling between yaw and pitch motion if the missile is not rolling. Therefore, it is imperative that the autopilot ensures zero roll angle of the missile. Once that is achieved, motion in yaw and pitch plane can be controlled independently. Therefore, it is enough to implement three PID controllers. One PID controller to ensure roll stability and two PID controllers for two lateral accelerations. Figure 2 shows a roll controller design.

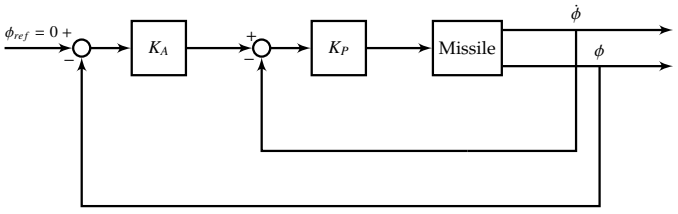

Figure 2: Roll controller design

Roll controller employs a cascade error regulation. The inner loop which feeds back roll derivative is a damping loop which ensures minimum oscillations in the roll channel. In order to achieve lateral acceleration tracking, an expression for calculating lateral acceleration is needed. In order to calculate them, a derivative of a rotating vector is needed and that vector has to be transformed into coordinate system whose x-axis coincides with the velocity vector. Such coordinate system is also called the wind frame. Therefore, accelerations in the wind frame are given by:

$$\begin{bmatrix} a_x \\ a_y \\ a_z \end{bmatrix} = \begin{bmatrix} \cos\alpha\cos\beta & -\sin\beta & \sin\alpha\cos\beta \\ \sin\beta\cos\alpha & \cos\beta & -\sin\alpha\sin\beta \\ -\sin\alpha & 0 & \cos\alpha \end{bmatrix} \left(\begin{bmatrix} \dot{u} \\ \dot{v} \\ \dot{w} \end{bmatrix} + \begin{bmatrix} P \\ Q \\ R \end{bmatrix} \times \begin{bmatrix} u \\ v \\ w \end{bmatrix} \right) \tag{17}$$

Where a_y and a_z are missile horizontal and vertical acceleration components normal to the velocity vector and a_x is the missile acceleration component along the velocity vector. This acceleration is usually zero since the missile does not have any fuel left during the terminal guidance phase. Figure 3 shows a controller for lateral accelerations. Similar design for horizontal and vertical acceleration components is employed. The inner loop reduces response oscillations and the outer loop ensures that the lateral acceleration follows the demanded lateral acceleration.

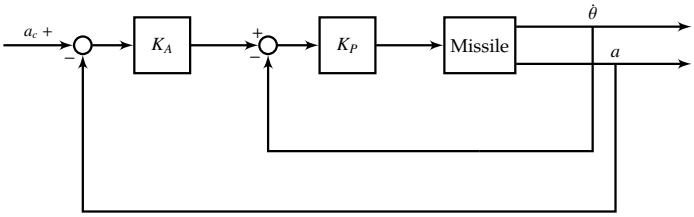

Figure 3: Lateral acceleration controller design

Missile aerodynamics coefficients change with respect to the Mach number, angle of attack, angle of sideslip, altitude and angular velocities, so it might be advisable to design multiple controllers for various operating points. This approach is referred to as gain scheduling [26, 27]. In his article fixed gain linear (PD) controllers are used regardless of missile homing operational conditions, due to their simplicity and robustness.

5. YOLO neural network

In order to calculate the tracking errors ϵ_y and ϵ_z, it is first required to localize object in the image. Furthermore, it is needed to classify the object in the obtained image. There is a handful of requirements that the localization algorithm

has to satisfy in missile guidance applications. First, during simulations images are obtained from Unreal Engine environment so the algorithm must be able to work with artificial images. Second, the algorithm has to be very fast since camera can generate images with very high frequency. Most suitable localization algorithm in this case is You Only Look Once(YOLO) convolutional neural network. YOLO was first introduced in 2016 where object detection was reframed as a single regression problem straight from image pixels to bounding box and class probabilities [9]. This made sure that YOLO needed only one passage through the network to obtain localization result which made it much faster then existing algorithms which were based on region proposals. Over time, a number of object detectors based on YOLO were developed. Most notably, YOLO9000 [28], YOLOv3 [29] and YOLOv4 [30] and YOLOv8 [31]. This article uses YOLOv4 since it is latest available in Matlab. YOLOv4 in Matlab is pretrained on Common Objects in Context(COCO) dataset [32] which consists of 80 classes and over 330000 images.

6. Camera model

Let us assume the pinhole camera model as is shown in the Figure 4 [33].

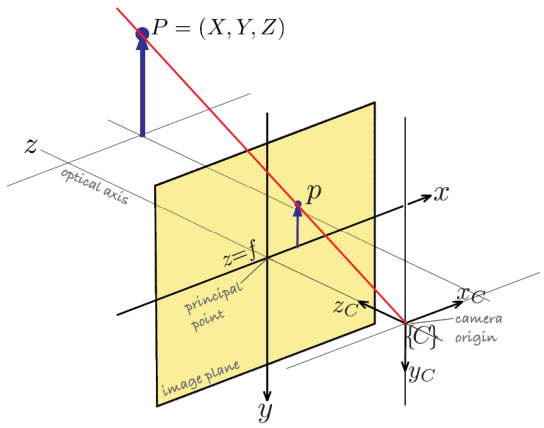

Figure 4: Pinhole camera model

Let X and Y denote the object size and let x and y denote size of the image in the image plane. Let f_x and f_y denote horizontal and vertical focal length measured in pixels which is also the distance of image plane from the CCD sensor. Inspecting Figure 4, it can be seen that tracking error angle in vertical plane can be evaluated as follows:

$$\epsilon_z = \arctan \frac{y}{f_y} \tag{18}$$

For vertical tracking error angle, the equation is analogous:

$$\epsilon_y = \arctan \frac{x}{f_x} \tag{19}$$

It is straightforward to implement calculation of the tracking errors. YOLO detector can obtain bounding box around the detected target with coordinates of the upper left corner(denoted with x_t and y_t) and its width and height(denoted with w and h). Now expressions for vertical and horizontal tracking errors are as follows:

$$\epsilon_z = \arctan \frac{y_t + h/2}{f_y} \tag{20}$$

$$\epsilon_y = \arctan \frac{x_t + w/2}{f_y} \tag{21}$$

7. Seeker camera gimbal servo controls

The camera is mounted on the head of the missile and it can rotate about the vertical and the horizontal axes on gimbal (yaw, pitch) using two DC motors. Rotational motions of these two motors is independent. Figure 5 shows mechanical structure of a missile seeker.

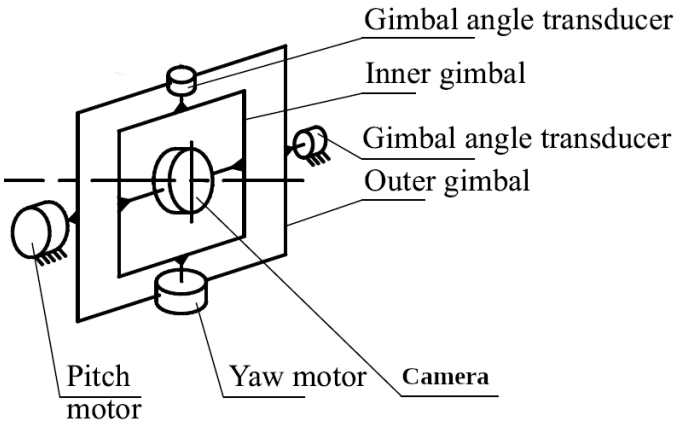

Figure 5: Seeker gimbal mechanical structure

The goal of these DC motor based servo systems is to nullify the tracking error so that the target is always at the center of the obtained image. Therefore, the target tracking problem can be viewed as a control problem where the tracking error is considered an output value with desired reference value equal to zero. This way, radome refraction error is minimized and better measurements are available. It is important to note that the gimbal servo control systems have to be sufficiently fast in order to quickly eliminate tracking errors. The servo motor can be modeled as a second order linear system as follows:

$$G(s) = \frac{\omega_n^2}{s\,(s + 2\xi\omega_n)} \tag{22}$$

Where ξ and ω_n are damping coefficient and system angular frequency respectively. The tracking loop dynamics bandwidth is very wide, usually about 100 rad/sec [10]. A standard PID controller is used for each gimbal axis. The controllers are tuned so that they achieve acceptable settling time and overshoot.

8. Missile guidance system synthesis

Each previous section presents a single part of the missile guidance system. The typical missile guidance system consists of guidance system, missile seeker, autopilot and

the missile itself. Figure 6 shows the block diagram of the missile guidance system.

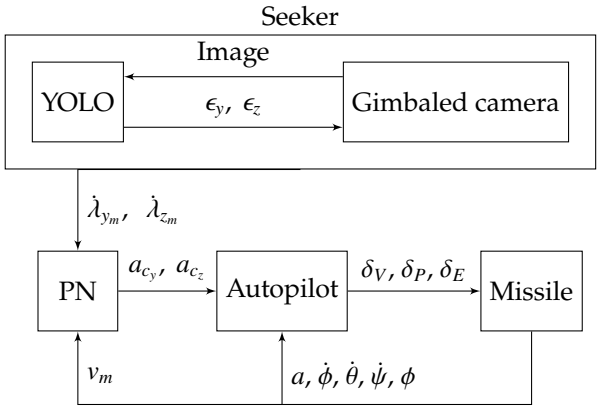

Figure 6: Missile guidance system design

Missile guidance systems design showed in the figure 6 only measures the image of the target. The remaining measurements can be obtained from the missiles internal sensors. Missile linear and angular velocities can be measured using inertial measurement units (IMU), from which Euler angles and their derivatives can be obtained using sensor fusion technique. Gimbal angles are measured by appropriate angle transducers.

9. Simulation

Previously described missile guidance system was implemented in Matlab and Simulink implementing previously described equations. Missile and the target position and orientation are fed into Unreal Engine blocks. Matlab offers Simulation 3D camera block to obtain images from the Unreal Engine scene. Simulation 3D camera block outputs an image which is fed to the YOLO block(implemented as a Matlab system) which calculates tracking errors given by equations 18 and 19. Camera generates 100 frames per second(fps) which is fast enough to capture tracking error dynamics. Obtained tracking errors are then fed into two PID controllers as error inputs. Controller outputs are fed into gimbal systems as inputs and gimbal positions are fed into camera as inputs to rotate the camera relatively to the missile body. Based on the equation 15, the seeker subsystem estimates the line of sight angular rate in the vertical and the horizontal plane. Subsystem for proportional navigation calculates the required lateral accelerations in vertical and horizontal plane. The autopilot subsystem calculates required elevator, rudder and aileron deflections.
Figure 7 shows trajectories of the target and the missile during the terminal guidance phase. The target is at the initial relative height of 200 meters and an initial relative distance of 500 meters. The target is escaping with the velocity 100m/s and moving sideways with the velocity 20m/s. It can also be seen that the missile is aiming at future intercept point rather than following the target. This means that PN requires lower commanded acceleration comparing to more traditional guidance methods.
Figure 8 shows one frame which is processed by YOLO detection algorithm. Here it can be seen that YOLO finds the bounding box around the object and that the object is in the center of the image.

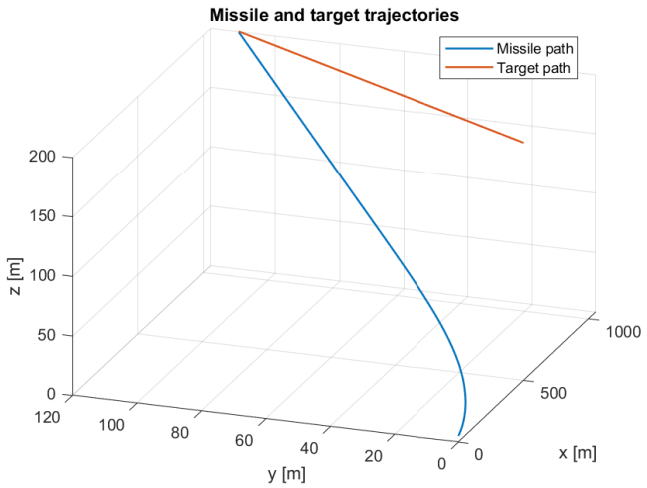

Figure 7: Missile and the target trajectories

Figure 8: Example of one image frame

Figure 9 shows obtained tracking errors. It can be seen that there are some initial oscillations due to the target moving which can be interpreted as output disturbances in the tracking errors.
Figures 10 and 11 show estimated and real LOS rates in the vertical and the horizontal plane respectively. It can be seen that the seeker estimates LOS rates fairly quickly and that they approach zero as the distance shortens which is a requirement for interception.
Figure 12 shows the missile Euler angles. It can be seen that the roll angle is always zero because the roll controller stabilizes the missile roll channel. The autopilot steers the missile so the missile has to keep an almost constant yaw and pitch angle in order to achieve a hit.
Figures 13 and 14 show commanded and achieved lateral accelerations. It can be seen that the autopilot subsystem ensures that the missile lateral accelerations are equal to the demanded PN accelerations.

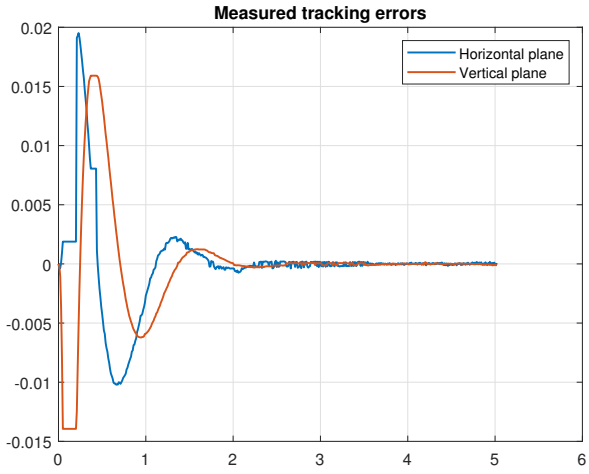

Figure 9: Tracking errors

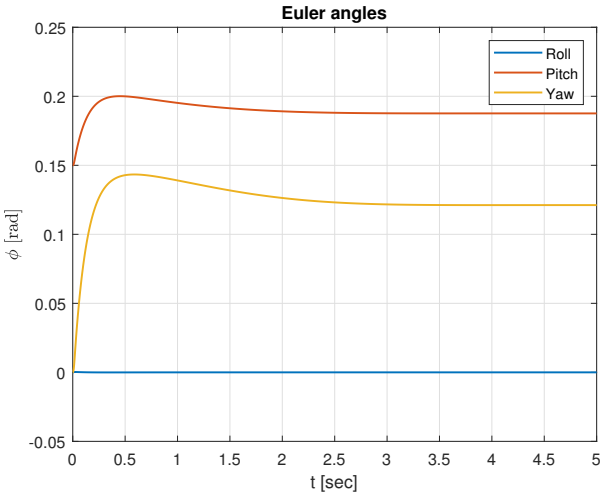

Figure 12: Missile Euler angles

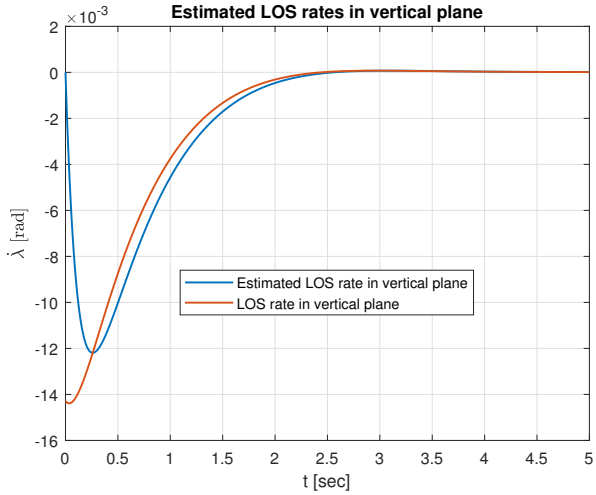

Figure 10: Estimated LOS rate in vertical plane

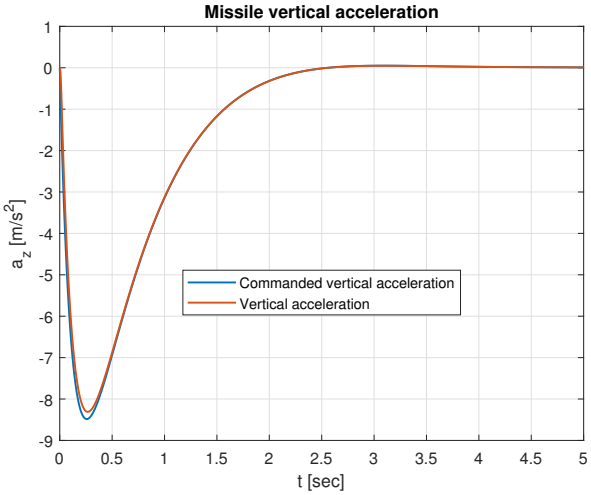

Figure 13: Missile vertical lateral acceleration

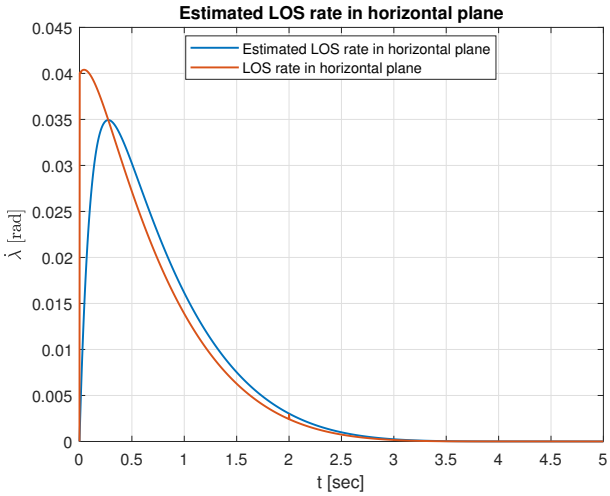

Figure 11: Estimated LOS rate in horizontal plane

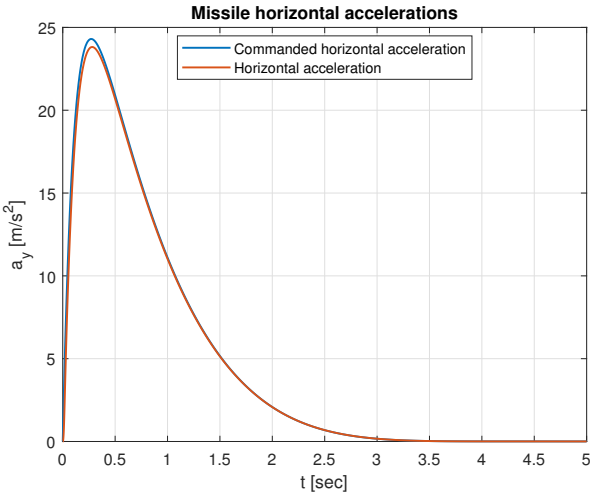

Figure 14: Missile horizontal lateral acceleration

Table 2: Missile performance table

Initial yaw heading error	Initial pitch heading error	Target horizontal acceleration	Target vertical acceleration	Miss distance	Maximum required horizontal acceleration	Maximum required vertical acceleration
−0.15 rad	0.15 rad	0	0	0 m	1.0384 m/s^2	9.81 m/s^2
−0.15 rad	0.3 rad	0	0	0 m	1.2325 m/s^2	9.6998 m/s^2
0 rad	0 rad	0.15g	0	0 m	1.8232 m/s^2	43.6711 m/s^2
0 rad	0 rad	0.3g	0	0 m	3.6392 m/s^2	43.6711 m/s^2
0 rad	0 rad	0.45g	0	0 m	5.4415 m/s^2	43.6711 m/s^2
0 rad	0 rad	0.6g	0	2.7509 m	7.2246 m/s^2	43.6711 m/s^2
0 rad	0 rad	0	0.15g	0 m	22.7714 m/s^2	43.6562 m/s^2
0 rad	0 rad	0	0.3g	0 m	23.2802 m/s^2	43.6562 m/s^2
0 rad	0 rad	0	0.45g	13.3609 m	23.2802 m/s^2	43.6562 m/s^2

10. Performance analysis

Proportional navigation can guarantee interception of a target moving with constant velocity. If the target is maneuvering or accelerating, there can be nonzero miss distance. Proportional navigation can ensure interception even if there is an initial heading error, although this requires the missile to have more energy available and larger demanded accelerations. Table 2 shows performance for various heading errors and target accelerations. Final miss distance and maximum required accelerations are chosen as a measure of performance. It can be seen that proportional navigation can nullify the miss distance due to the initial heading error given that the missile can achieve demanded lateral acceleration. If the target is accelerating, the proportional navigation may not be able to nullify the miss distance.

11. Conclusion

This article presents design and simulation of missile homing system. The missile homing system consist of guidance law, autopilot and imaging based target tracking subsystem (missile seeker). In this work the guidance law is based on true proportional navigation. Autopilots stabilize roll angle and regulate horizontal and vertical accelerations. They are standard linear multi loop controllers. Two axes (pitch, yaw) gimbaled seeker use standard PID controllers to track the target. The seeker uses state-of-art deep machine learning YOLO (You Only Look Once) object detector for tracking error measurements and LOS rate estimation. Comprehensive homing missile simulator is developed, and simulation results show robust accuracy of the proposed scheme to target velocity, launch heading errors and low level target maneuvering. Our future research work will focus on design and simulation of advanced guidance and control laws, as well as design and simulation of advanced machine learning algorithms.

References

[1] M. Abd-elatif, L. jun Qian, Y. ming Bo, "Optimization of three-loop missile autopilot gain under crossover frequency constraint", *"Defence Technology"*, vol. 12, no. 1, pp. 32–38, 2016, doi:https://doi.org/10.1016/j.dt.2015.08.006.

[2] B. Zhang, Q. Lv, Y. Lei, "The application of pid controller in missile longitudinal loop system and its simulation", *"Proceedings of the 5th International Conference on Advanced Design and Manufacturing Engineering"*, pp. 2113–2118, Atlantis Press, 2015/10, doi:10.2991/icadme-15.2015.395.

[3] A. Awad, H. Wang, "Roll-pitch-yaw autopilot design for nonlinear time-varying missile using partial state observer based global fast terminal sliding mode control", *"Chinese Journal of Aeronautics"*, vol. 29, no. 5, pp. 1302–1312, 2016, doi:https://doi.org/10.1016/j.cja.2016.04.020.

[4] A. Thukral, M. Innocenti, "A sliding mode missile pitch autopilot synthesis for high angle of attack maneuvering", *"IEEE Transactions on Control Systems Technology"*, vol. 6, no. 3, pp. 359–371, 1998, doi:10.1109/87.668037.

[5] C.-D. Yang, C.-C. Yang, "A unified approach to proportional navigation", *"IEEE Transactions on Aerospace and Electronic Systems"*, vol. 33, no. 2, pp. 557–567, 1997, doi:10.1109/7.575895.

[6] S. A. Murtaugh, H. E. Criel, "Fundamentals of proportional navigation", *"IEEE Spectrum"*, vol. 3, no. 12, pp. 75–85, 1966, doi:10.1109/MSPEC.1966.5217080.

[7] M. Guelman, "A qualitative study of proportional navigation", *IEEE Transactions on Aerospace and Electronic Systems*, vol. AES-7, no. 4, pp. 637–643, 1971, doi:10.1109/TAES.1971.310406.

[8] M. Guelman, "Proportional navigation with a maneuvering target", *"IEEE Transactions on Aerospace and Electronic Systems"*, vol. AES-8, no. 3, pp. 364–371, 1972, doi:10.1109/TAES.1972.309520.

[9] J. Redmon, S. Divvala, R. Girshick, A. Farhadi, "You only look once: Unified, real-time object detection", *https://arxiv.org/abs/1506.02640*, 2016.

[10] G. M. Siouris, *Missile Guidance and Control Systems*, Springer-Verlag New York, 2004.

[11] J. Harris, N. Slegers, "Performance of a fire-and-forget anti-tank missile with a damaged wing", *"Mathematical and Computer Modelling"*, vol. 50, no. 1, pp. 292–305, 2009.

[12] U. Shukla, P. Mahapatra, "The proportional navigation dilemma-pure or true?", *"IEEE Transactions on Aerospace and Electronic Systems"*, vol. 26, no. 2, pp. 382–392, 1990.

[13] M. Hodžić, N. Prljača, "Simulation of short range missile guidance using proportional navigation", *"2021 20th International Symposium INFOTEH-JAHORINA (INFOTEH)"*, pp. 1–6, 2021.

[14] M. Hodžić, N. Prljača, "Los rate estimation techniques for proportional navigation guided missiles", *"2022 21st International Symposium INFOTEH-JAHORINA (INFOTEH)"*, pp. 1–6, 2022.

[15] P. Zarchan, *Tactical and Strategic Missile Guidance*, no. v. 219 in AIAA Tactical Missile Series, American Institute of Aeronautics and Astronautics, 2007.

[16] R. Yanushevsky, *Modern Missile Guidance*, Taylor & Francis, 2007.

[17] N. Shneydor, *Missile Guidance and Pursuit: Kinematics, Dynamics and Control*, 1, Elsevier Science, 1998.

[18] M. Drela, *Flight Vehicle Aerodynamics*, FLIGHT VEHICLE AERODYNAMICS, MIT Press, 2014.

[19] S. Graovac, *Automatsko vođenje objekata u prostoru*, Akademska Misao, 2005.

[20] C.-F. Lin, *Modern Navigation, Guidance and Control Processing*, Prentice Hall, 1991.

[21] M. V. Cook, ed., *Flight Dynamics Principles (Third Edition)*, Butterworth-Heinemann, third edition ed., 2013.

[22] N. F. Palumbo, R. A. Blauwkamp, J. M. Lloyd, "Basic principles of homing guidance", *"Johns Hopkins Apl Technical Digest"*, vol. 29, pp. 25–41, 2010.

[23] Q. Zaikang, L. Defu, *Design of Guidance and Control Systems for Tactical Missiles*, CRC Press, 1st ed., 2019.

[24] S. Mondal, S. Sadhu, A. Banerjee, "Platform motion disturbances attenuation in a missile seeker subsystem using internal model control", *"2013 International Conference on Control, Automation, Robotics and Embedded Systems (CARE)"*, pp. 1–4, 2013.

[25] S. He, Y. Liang, J. Tang, Z. Bai, K. Li, "Homing guidance law design against maneuvering targets based on ddpg", *"International Journal of Aerospace Engineering"*, vol. 2023, p. 4188037, 2023.

[26] D. White, J. Wozniak, D. Lawrence, "Missile autopilot design using a gain scheduling technique", *"Proceedings of 26th Southeastern Symposium on System Theory"*, pp. 606–610, 1994.

[27] A. Hiret, G. Duc, J. Bonnet, "The application of gain-scheduling h controllers for a missile autopilot", *"IFAC Proceedings Volumes"*, vol. 31, no. 21, pp. 59–64, 1998, 14th IFAC Symposium on Automatic Control in Aerospace 1998, Seoul, Korea, 24-28 August 1998.

[28] J. Redmon, A. Farhadi, "Yolo9000: Better, faster, stronger", *https://arxiv.org/abs/1612.08242*, 2016.

[29] J. Redmon, A. Farhadi, "Yolov3: An incremental improvement", *https://arxiv.org/abs/1804.02767*, 2018.

[30] A. Bochkovskiy, C.-Y. Wang, H.-Y. M. Liao, "Yolov4: Optimal speed and accuracy of object detection", *https://arxiv.org/abs/2004.10934*, 2020.

[31] D. Reis, J. Kupec, J. Hong, A. Daoudi, "Real-time flying object detection with yolov8", 2023.

[32] T.-Y. Lin, M. Maire, S. Belongie, L. Bourdev, R. Girshick, J. Hays, P. Perona, D. Ramanan, C. L. Zitnick, P. Dollár, "Microsoft coco: Common objects in context", *https://arxiv.org/abs/1405.0312*, 2015.

[33] P. Corke, *Robotics, Vision and Control - Fundamental Algorithms in MATLAB®*, vol. 73 of *Springer Tracts in Advanced Robotics*, Springer, 2011.

MIRZA HODŽIĆ was born in Tuzla, Bosnia and Herzegovina in 1997. He finished his bachelor's degree from the Faculty of electrical engineering in Tuzla in 2020. He has done his master's degree from Faculty of electrical engineering Tuzla in 2022 at the department of control systems and robotics. Besides working in the industry he is also working at the Faculty of electrical engineering at the department of control systems , robotics and industrial informatics. His research interests are in robotics, control systems, machine vision and missile guidance. Currently, he is working on his PhD in control systems at the Faculty of electrical engineering at the University of Tuzla.

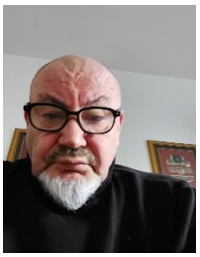

NASER PRLJAČA is full professor and head of department of Control Systems, Robotics and Industrial Informatics at the Faculty of Electrical Engineering, University of Tuzla. He holds BSc, MSc and PhD in Electrical and Electronics Engineering. He has been taking part in numerous research and industrial projects, and is author of a number of academic publications. His research and teaching interests include control systems, embedded systems, robotics, machine learning and computer vision.

JENRS

Received: 04 February, 2024, Revised: 08 March, 2024, Accepted: 11 March, 2024, Online: 31 March, 2024

DOI: https://doi.org/10.55708/js0303004

Asthma Monitoring Systems Based on Electro-Infrared Sensors: A Review

Auns Qusai Al-Neami[1], **Zina Ali Abed**[*, 2]

[1] Biomedical Engineering Department, College of Engineering, Al-Nahrain University, Baghdad, Iraq

[2] Medical Instrumentation Engineering department, Medical Technical College, AL-Farahidi University, Baghdad, Iraq

*Corresponding author: Zina Ali Abed, Baghdad, Iraq, 009647827120909, eng.zinaali@gmail.com

ABSTRACT: Asthma is one of the chronic diseases that affected on the respiratory system. Studies had showed that more than 350 million people who suffering from asthma around the world which is equivalent to 1 in each 12 adults. Many intelligent monitoring systems had proposed in order to help the patient to know the situation before the frenzy happens. This approach has additionally been applied by individuals wanting to boost the standard of life by utilizing this technology. This paper tends to perform a comprehensive coverage and review that aim to show and analyze the advances of the most recent studies supported medical aid in the field of respiratory system especially monitoring and detection of the asthma disorder based on infrared sensors. The present analysis covers revealed manuscripts in scientific journals and recognized conferences since the year 2016. Also, it tends to show a reference model supported the analysis of the resources used from the chosen studies. Finally, the objective of the present proposal is to assist future enthusiasts to get and enumerate the specified factors related with asthma monitoring systems based on infrared sensors.

KEYWORDS: Respiratory system, Asthma monitoring systems, Chronic disease, Infrared sensors.

1. Introduction

The most important parameter in the human lungs is the Carbon Dioxide (CO_2) concentration, this measurement called capnogram. Which was first measured in the early 1900s [1, 2]. The concentration of the CO_2 can be measured accurately by using capnogram, Also its features use to provide overall information about Chronic Pulmonary Disease in addition to cardiorespiratory disorders, Congestive Heart Failure, and asthma [3-5]. Nowadays, asthma consider as one of the most threated diseases of respiratory disorders. in the world, Asthma considered as the fourteenth rank of the most common respiratory disorders. About 334 million people affected by asthma around the world, 9% from them are adult while children represent 14% of them [4, 6, 7]. In Malaysia, 10-13% of population affected by Asthma, While in Malays 67% of population affected by this disease, In Chinese and Indians the percentage goes from 7.3% to 12.9% respectively [8, 9]. The devices that used to diagnosis asthma are patient dependent device, which they require co-operation from patients, so it's difficult to use by children. Therefore, an independent device used to diagnosis asthma must be exist, for example, capnography in order to assess the respiratory the function of asthmatics [10-12]. Many devices were developed to make the diagnosis and monitoring of asthma easier such as Spirometer and peak flow meter. Hence, many studies were carried out in Google Scholar between 2010 to 2023 by utilizing standard English language, By using different keywords such as (capnogram, infrared sensor, asthma monitoring system, CO_2 sensor, respiratory CO_2, capnogrph, and monitoring system) to define CO_2 sensors technology, and capnogram features [13-15].

The concentration of exhaled carbon dioxide was measured by using end-tidal CO_2 ($ETCO_2$) detectors. The end-tidal CO_2 represent the partial pressure or maximal concentration of CO_2 at the end of exhalation. Which is correlates to the arterial concentration of CO_2 in patient [16]. Different design of the detectors are introduce along the time, But overall quantitative and qualitative Detectors can be considered as the main type of capnograph [17]. If the detector use to detect the presence or absent of the CO_2, it's a qualitative detector such as colorimetric detector which indicate the absent or present of the CO_2 in exhaled

gas by using color. More detailed information given by using the quantitive detector because it read the level of CO_2 in the exhaled gas [18-20]. Another classification of the detector depend on Their location in the airway system divide into mainstream and sidestream devices, IR sensor (Infrared sensor) are a Mainstream detectors where gas flow goes directly into the device to produced real-time wave of the CO_2 waveform. Which is used mainly with intubated patients. While Sidestream detectors are located away from the path of air flow in the respiratory system. Such as Nasal monitoring of end-tidal CO_2 [21, 22].

Capnography used in patients through anesthesia, ventilator cases, and head trauma. But its main benefit used in intubated patients, Also it can be used in patients that are awake in children and adult [23, 24]. By using a sidestream capnograph attached to a nasal catheter produced $ETCO_2$ values that correlated well with $PaCO_2$ readings capnography could be used attached to a facemask [25-28].

The main different between mainstream and sidestream are shown in table 1 and figure 1. witch represent the different in definition of the names, the effect of the environment on the reading to show that mainstream capnogram has un issue by mixing the sample gas which will effect on the reading, While the sidestream capnogram has delay time results from remote location. Also the table and figure show the different in the main parts of each devices and give the end result of each device.

Table 1: Comparison Between Mainstream and sidestream capnography [21, 27, 29, 30]

Mainstream	**Sidestream**
Name as Non-Diverting capnometer measuring CO_2 concentration away from the patient airway.	Name as Diverting capnometer measuring CO_2 concentration at the patient airway.
Issue of the mainstream capnometer include different in temperature and humidity between sampling site and monitor site, removal of water through the distance, the sample gas may mix through the cell which will affect on the reading, pressure drop across the tubing, and dynamic distortions to the waveform	Issue of the sidestream capnography include delay time results from using a remote location, this delay may last for up to several seconds with 200ms distortion the total response time (delay) can be useful to provide time for the clinician to prepare for the patient's case
It consists from the sample cell and infrared bench	It consists of 6- to 8-foot-long small-bore tube with water trap and drying tubing and sample cell
Give a real-time reading of the partial pressure of CO_2 (carbon dioxide) within the respiratory system	To aspirate a sample of gas from the breathing circuit in the respiratory through a 6- to 8-foot-long small-bore tube at a flow rate that may vary as much as ±20%

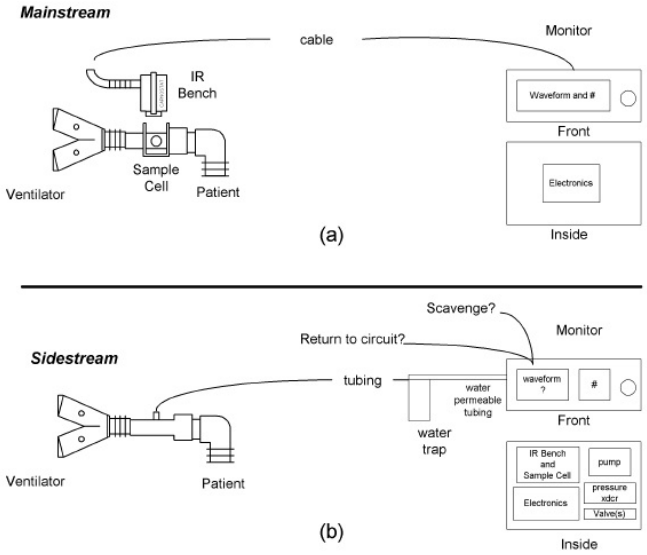

Figure 1: The main difference between Mainstream and Sidestream Capnograph for breathing circuit [21]

2. Related Work

In 2013, the authors made a comparison between mainstream and sidestream measurement of end tidal carbon dioxide ($PETCO_2$) was made by taking 114 subjects which was patients require arterial blood gas analysis, By using Bland-Altman method (it's a method used to calculates the mean difference between two methods of measurement (the 'bias')) to evaluate between the $PETCO_2$ measurements and $PaCO_2$ measurement witch represent the measures of an arterial blood gases (ABG) to evaluates carbon dioxide (CO_2) levels in the blood. It results in the mainstream, 13mm Hg value different between $PETCO_2$ and $PaCO_2$ (0.6 to 25.5 agreement limits to 95%) with moderate correlation ($P < .001$, r 0.55). While in the sidestream 9.7 mm Hg value difference between $PETCO_2$ and $PaCO_2$ (5.4 to 24.7 agreement limits to 95%) with poor correlation ($P < .001$, r 0.41). that improve $PETCO_2$ has lower value than the $PaCO_2$ [26].

In 2016, the authors had proposed a continuous monitoring system that helps asthmatics to monitor the activity of their lungs as well as the related environmental parameters. Asthma symptoms can be detected by using this monitoring system. The designed system consists of a device module to monitor the temperature, humidity,

activity, air pressure and the flown gases that surround asthmatics patient. The data then sent from the device to the patient's doctor by using a Global System for Mobile Communication (GSM). The doctor could examine the sensed values and he could take the desired decision for giving the asthmatics the right treatment and medications. This proposed system is low cost, credible, and friendly to use in order to find out the asthma symptoms in asthmatics [31]. In 2017, the authors had developed a smart model of asthma prediction system using Internet since there are 334 million people around the world are suffering from asthma. Asthmatics are sensitive to things that may not bother the normal people, they feel uncomfortable when the level of smoke increased, either fog or pollution in the surrounding air. The number of asthmatics has been increasing so fast over the years. The developed model helps to prevent asthma from happen by detecting the causes of asthma [32]. In 2018, the authors made a review study investigate, and compare between different infrared carbon dioxide sensors specifications, this study also gives the capnogram features that use to develop an asthma-monitoring device. The keywords used was (infrared sensor, CO_2 sensor, capnograph, CO_2 measurement, capnogram, and asthma detection) by using PubMed, Google Schooler, scoups and another search engine. The COMET (COMET is the name of the company made the sensor) carbon dioxide sensor distinguish as the most suitable and reliable sensor proper for asthma diagnosis and monitoring according to this study, this device was chosen from other based on its weight (7 g), warm-up time (2-15s), output range (0-99 mmHg), and response time (0.028 s). Furthermore, to screen asthma severity level, slope and time-frequency components must be measured from alveolar phase and complete breath cycle respectively [33]. In 2018, the authors made a Narrative Review on the Applications of End-Tidal Carbon Dioxide ($ETCO_2$) Monitoring in Emergency room was made by using PubMed, Scopus, Cochrane Databases, and other search engine by using keywords like emergency department monitoring, $ETCO_2$, and critical monitoring. In this study capnography was use to measure many clinical cases. It's use to measure $ETCO_2$ as an precise method that use to help in emergency cases. But this device is not used in all emergency cases and not used regularly. it's usually used in patients under sedation (Anesthesia) or connected to mechanical ventilation, patient suffering from shock, heat dropping due to pulmonary disease, patient who suffering from metabolic disorder, or has trauma. Which is means that capnography considered as an essential tool in emergency department [34].

3. Methodology

Depending on the introduction, we propose a review for home-based and handheld monitoring system capnograph device [3, 35, 36]. The main objective of this study is to show the best device that has the ability to monitor asthma in the home environment and assists in the progression and handling of asthma which is the COMET CO_2 sensor [5, 37, 38]. Till now, too many studies have made huge steps towards the monitoring and detection of cardio-respiratory conditions and disorders, specifically, asthma, this is done by using a capnography [32, 39]. The schematic block diagram in figure 2 shows the proposed system in the present study for monitoring asthma and also it determines the lung disease in asthmatics.

This system measures several parameters because the device is dealing with air so the Humidity, pressure, Airflow, voltage, temperature, and CO_2 concentration sensors represent the main feature of the air breathed that need to be monitor for example if the humidity of the air was too high it will cause suffocation of the patient and increase the illness, each active sensor then connected to a microcontroller (Raspberry Pi was use because the code of the program was written by python language to made the program more freely to edited from other language) which is supplied by line power or battery then the processed signal display on mobile communication which has GPS locater, Bluetooth module and GSM (Global System for Mobile Communications). The data that sent to mobile communication module interfaced to the specialist to make the correct examination in medications and treatment for the patient. This monitoring system is friendly to use by patient, economic. The CO_2 sensor module in which the signal conditioning (the electronic circuit that use to enhance and manipulate the signal to the desire output needed from the next process) down is shown in figure 3 [40-42].

The microcontroller also sends the data to CO_2 gas concentration to determine the concentration of the exhaled CO_2 and then display it on LCD monitor.

4. Results

As the aim of this study is to make a full review and comparison among the infrared CO_2 sensors multiple specifications and others to develop an efficient asthma monitoring device. As shown in Table 2 and 3 the specification of COMET CO_2 sensor which indicate that this sensor is the most reliable sensor used to assess the asthma. Moreover, time-frequency components and the slope which measured from the overall respiratory cycle and alveolar phase; which is found the most important

features to show the seriousness level of asthma. The feedback was done at a constant temperature (25°C) discovers that the carbon dioxide values are totally changed as (17,835.19-86,321.29) parts per million (ppm) whenever the pressure changed as (16.53-81.53) kPa. These measurements have. The sensors measurements are illustrated in figures (3), (4), and (5).

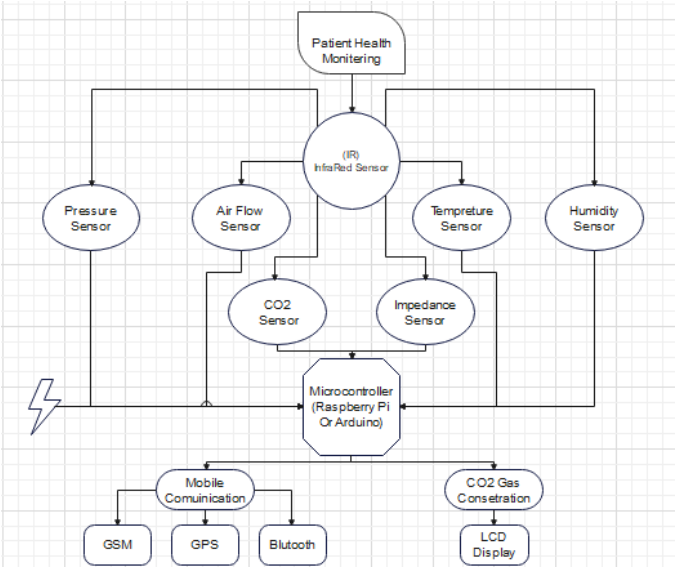

Figure 2: The Proposed Schematic Block Diagram of Asthma Monitoring System in the Present Study.

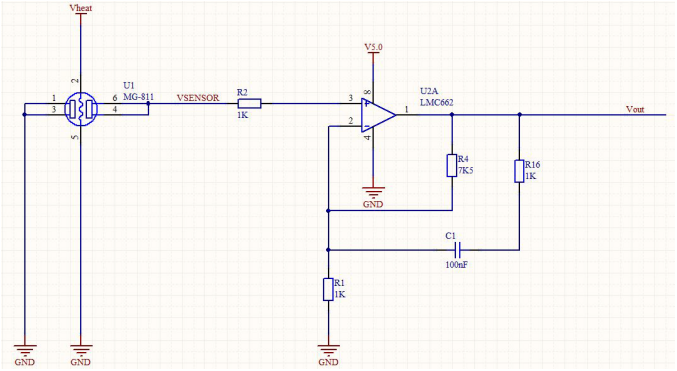

Figure 3: CO_2 Sensor Module [40, 43]

Table 2: CO_2 Infrared Sensor Specifications [44, 45]

Sensor Parameter	Specifications
Weight in gram	7 g
(Tr) Response Time	0.028 s
Pressure Output Range	0-99 mmHg
(Tw) Warm-up Time	2-15 s

The line graph responses of three different CO_2 sensors show that the COMET I and II types are the best types of the CO_2 sensors. In figure 4 these lines graph is color coded. the blue line represents the temperature which was fixed at 25°C, the orange line represents the relative humidity which is approximately between 14-24% of the air, the green line represents the Dew point between -7 to 0.8, The red line represents the CO_2 level while the pink line represents the maximum limit can the result reach. In figure 5 represent the most turbulence area zoomed from figure 4 and show all the label with reading on the graph.

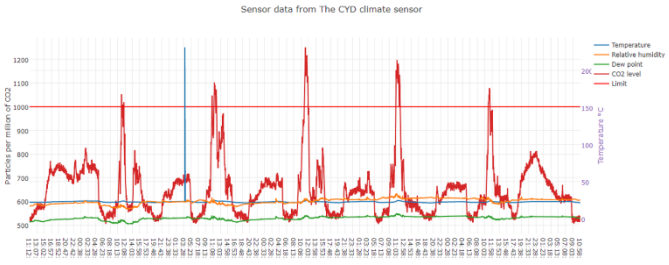

Figure 4. The Line Graph Response of COMET-I, II CO_2 Sensors [46,47].

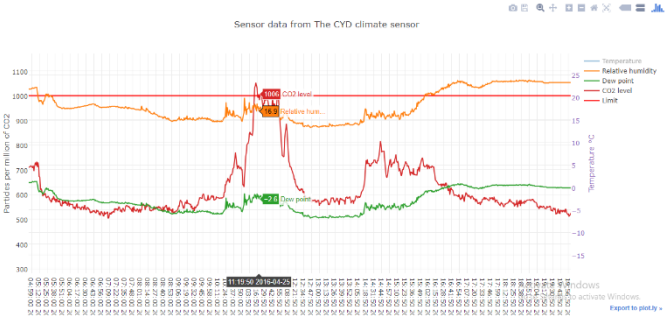

Figure 5. The zoomed Line Graph Response of COMET-I, II CO_2 Sensors which show the pointer give the read of CO2 level, the relative Humidity and Dew point [46, 47].

In figure 6 and 7 show the different between the line graph of real and digital CO_2 sensors it shows that the real CO_2 sensor react as a U shape curve while the digital CO_2 sensor act as downward slope to infinity because in digital CO_2 many parameters were neglected like the temperature and humidity.

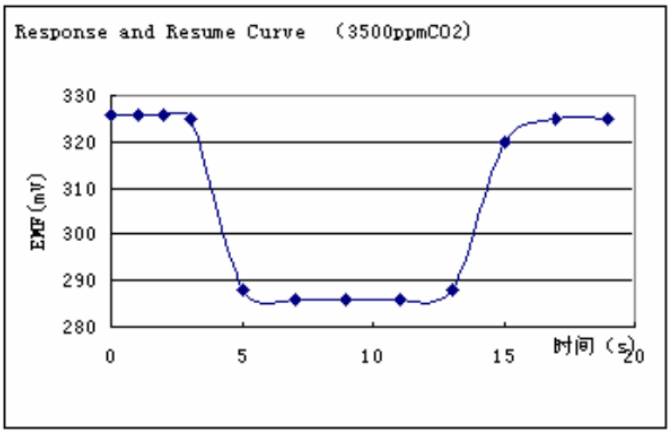

Figure 6: The Line Graph Response of CO2 Sensor 27929 [48].

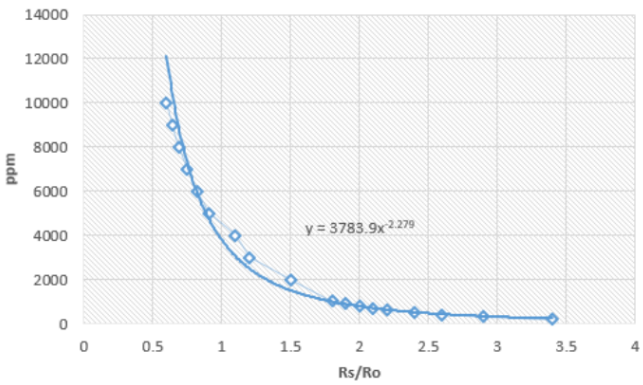

Figure 7: The Line Graph Response of Digital CO2 Sensor EE893 [13].

Conclusion

The proposed paper gives overall investigations and also comparison between more than one research that were based on infrared CO_2 sensors. There are many specifications should be taken in considerations like, Temperature at the operating time, weight of the device that will be held by the patient, voltage at the operating time, approximate cost of the device, time that take the device to response to the signal, the time that the device needs to warm-up, the pressure output range, and the applications of the device. It was clear from this study that both the COMET one and two, Digital carbon dioxide (EE893) sensors and carbon dioxide (27929) are the most accurate and efficient for creating a home-made asthma monitoring system. Furthermore, these sensors measured the inspired CO_2, rate of respiration, $ETCO_2$ (end-tidal carbon dioxide), and TIME OF inspiration and expiration Therefore, by using the equivalent CO_2 sensors which is a light weight, hand-held, precise, and quantitative capnography device that designed and developed. for this reason, the lifetime of the pretended features when developing a canograph system or device should conform in future work.

Table 3: Different Types Infrared CO_2 Sensors and their Specification [49-52]

CO_2 Sensor	Operating voltage	Range (% CO_2)	Operating Temperature (°C)	Sensitivity/ Accuracy (%)	Application
COMET-I, II	5	0-13.8	5-55	±0.42%	Carbon dioxide partial pressure, end tidal ETCO2, Respiration Rate, inspired carbon
CO_2 Sensor 27929	6.5-12	0.035-1	0 to 70	High Sensitivity	alarm of over-limit Gas level; device; equipment of Environmental monitoring
Digital CO_2 Sensor EE893	4.75-7.5	0-0.2/0.5/1	40- to 60	0-0.2%: < ±(0.005% at ±2% of measuring value)	transmitters Data loggers; Wireless; Handhelds; Demand controlled ventilation Building management;

Weight/Size (Approx. in grams)	Approx. Cost (in$)	(Tw) Warm-up Time (s)	(Tr) Response Time (s)
<7.0	400	2-15	0.028
4	43.55	>20	>10
10	299	15	105

References

[1] M. S. Siobal, "Monitoring Exhaled Carbon Dioxide," (in eng), *Respir Care,* vol. 61, no. 10, pp. 1397-416, Oct 2016.

[2] S. S. Pandya NK. (Updated 2022 Aug 29). *Capnography And Pulse Oximetry*. Available: https://www.ncbi.nlm.nih.gov/books/NBK539754/

[3] M. B. Jaffe, "Using the features of the time and volumetric capnogram for classification and prediction," (in eng), *J Clin Monit Comput,* vol. 31, no. 1, pp. 19-41, Feb 2017.

[4] P. Ellwood *et al.*, "The Global Asthma Network rationale and methods for Phase I global surveillance: prevalence, severity, management and risk factors," (in eng), *Eur Respir J,* vol. 49, no. 1, Jan 2017.

[5] G. K. B.Abinayaa, B.Saranya, R.Gayathri, "An Intelligent Monitoring Device for Asthmatics using Arduino," *International Journal of Advanced Research in Electrical, Electronics and Instrumentation Engineering,* vol. 5, no. 7, 2016.

[6] O. Enilari and S. Sinha, "The Global Impact of Asthma in Adult Populations," (in eng), *Ann Glob Health,* vol. 85, no. 1, Jan 22 2019.

[7] S. C. Dharmage, J. L. Perret, and A. Custovic, "Epidemiology of Asthma in Children and Adults," (in eng), *Front Pediatr,* vol. 7, p. 246, 2019.

[8] I. f. P. Health, "The Third National Health and Morbidity Survey (NHMS III)," vol. 1, M. Ministry of Health, Ed., ed, 2006.

[9] C. Nickson. (2020). *Capnography Waveform Interpretation*. Available: https://litfl.com/

[10] K. Tan Teik and M. B. Malarvili, "Analysis of capnography for asthmatic patient," in *2009 IEEE International Conference on Signal and Image Processing Applications*, 2009, pp. 464-467.

[11] M. Cully, M. Treut, A. D. Thompson, and A. D. DePiero, "Exhaled end-tidal carbon dioxide as a predictor of lactate and pediatric sepsis," (in eng), *Am J Emerg Med,* vol. 38, no. 12, pp. 2620-2624, Dec 2020.

[12] David A. Wampler. (2011). *Capnography as a Clinical Tool*.

[13] B. A. a. A. A. Raja, "Smart Portable Monitoring Device for Asthma Patients," *Middle-East Journal of Scientific Research,* vol. 24 (S1), no. 1990-9233, 2016.

[14] E. Y. Rifky Maulana Fuadi, Bambang Guruh Irianto,Abhishek Mishra, "Design of Carbon Dioxide Levels Measurement in Human Expiration Using EtCO2 Capnography Method," *Indonesian Journal of Electronics, Electromedical Engineering, and Medical Informatics,* vol. vol. 5, pp. 45-47, 2023.

[15] G. Casey, "Capnography: monitoring CO2," (in eng), *Nurs N Z,* vol. 21, no. 9, pp. 20-4, Oct 2015.

[16] E. Razi, G. A. Moosavi, K. Omidi, A. Khakpour Saebi, and A. Razi, "Correlation of end-tidal carbon dioxide with arterial carbon dioxide in

mechanically ventilated patients," (in eng), *Arch Trauma Res,* vol. 1, no. 2, pp. 58-62, Summer 2012.

[17] S. Fan, Z. Li, K. Xia, and D. Hao, "Quantitative and Qualitative Analysis of Multicomponent Gas Using Sensor Array," vol. 19, no. 18, p. 3917, 2019.

[18] T. Nowicki, Z. Jamal, and S. London, "Carbon Dioxide Detector," in *StatPearls*Treasure Island (FL): StatPearls Publishing Copyright © 2023, StatPearls Publishing LLC., 2023.

[19] R. H. Friesen and M. Alswang, "End-tidal PCO2 monitoring via nasal cannulae in pediatric patients: accuracy and sources of error," (in eng), *J Clin Monit,* vol. 12, no. 2, pp. 155-9, Mar 1996.

[20] R. J. Mieloszyk *et al.*, "Automated quantitative analysis of capnogram shape for COPD-normal and COPD-CHF classification," (in eng), *IEEE Trans Biomed Eng,* vol. 61, no. 12, pp. 2882-90, Dec 2014.

[21] M. B. Jaffe, "Mainstream or Sidestream Capnography?," *Medical Device depot inc*.

[22] A. Conway, C. Douglas, and J. R. Sutherland, "A systematic review of capnography for sedation," (in eng), *Anaesthesia,* vol. 71, no. 4, pp. 450-4, Apr 2016.

[23] M. E. Stone, Jr. *et al.*, "End-tidal CO(2) on admission is associated with hemorrhagic shock and predicts the need for massive transfusion as defined by the critical administration threshold: A pilot study," (in eng), *Injury,* vol. 48, no. 1, pp. 51-57, Jan 2017.

[24] K. L. Chan, M. T. V. Chan, and T. Gin, "Mainstream vs. sidestream capnometry for prediction of arterial carbon dioxide tension during supine craniotomy," vol. 58, no. 2, pp. 149-155, 2003.

[25] C. Sumner. (2023). *Capnography*.

[26] O. C. Murat Pekdemir, Serkan Yılmaz, Elif Yaka and Melih Yuksel, "Disparity Between Mainstream and Sidestream End-Tidal Carbon Dioxide Values and Arterial Carbon Dioxide Levels," *Respiratory Care,* vol. 58(7), no. 1152-1156, 2013.

[27] M. Sakuraya *et al.*, "Accuracy evaluation of mainstream and sidestream end-tidal carbon dioxide monitoring during noninvasive ventilation: a randomized crossover trial (MASCAT-NIV trial)," *Journal of Intensive Care,* vol. 10, no. 1, p. 17, 2022/03/18 2022.

[28] T. M. G. P. Room. (2023). *Differences between Mainstream and Sidestream Capnography*. Available: http://www.meditech-egypt.com/Education/

[29] Capnomed, "Mainstream EtCO2 MODULE," ed, 2018.

[30] F. P. A.L.Balogh, G.H.Fodor, J.Tolnai, Z.Csorba and B.Babik, "Capnogram slope and ventilation dead space parameters :comparison of mainstream and sidestream techniques," *BritishJournalofAnaesthesia,* 2016.

[31] S. Zou, J. Zhang, and Z. Zhang, "A novel approach for predicting microbe-disease associations by bi-random walk on the heterogeneous network," *PLOS ONE,* vol. 12, no. 9, p. e0184394, 2017.

[32] S. Malik, O. P. Singh, A. Nurifhan, and M. Balakrishnan, *Portable Respiratory CO2 Monitoring Device for Early Screening of Asthma*. 2016.

[33] O. P. Singh and M. Balakrishnan, "Review of Infrared Carbon-Dioxide Sensors and Capnogram Features for Developing Asthma-Monitoring Device," *Journal of Clinical and Diagnostic Research,* vol. 12, pp. OE01-OE06, 10/01 2018.

[34] H. Aminiahidashti, S. Shafiee, A. Zamani Kiasari, and M. Sazgar, "Applications of End-Tidal Carbon Dioxide (ETCO2) Monitoring in Emergency Department; a Narrative Review," (in eng), *Emerg (Tehran),* vol. 6, no. 1, p. e5, 2018.

[35] O. P. Singh, I. M. El-Badawy, and M. Balakrishnan, "Design and validation of a handheld capnography device for cardiopulmonary assessment based on the Arduino platform," *Journal of Innovative Optical Health Sciences,* vol. 14, 04/27 2021.

[36] D. F. T. Morais, G. Fernandes, G. D. Lima, and J. J. P. C. Rodrigues, "IoT-Based Wearable and Smart Health Device Solutions for Capnography: Analysis and Perspectives," vol. 12, no. 5, p. 1169, 2023.

[37] B. E. Himes, L. Leszinsky, R. Walsh, H. Hepner, and A. C. Wu, "Mobile Health and Inhaler-Based Monitoring Devices for Asthma Management," (in eng), *J Allergy Clin Immunol Pract,* vol. 7, no. 8, pp. 2535-2543, Nov-Dec 2019.

[38] J. T. Oduor, "A Model for home-based remote monitoring of asthmatic patients ", Strathmore University, 2017.

[39] J. Prinable, P. Jones, C. Thamrin, and A. McEwan, *A novel hardware implementation for detecting respiration rate using photoplethysmography*. 2017, pp. 726-729.

[40] H. Abderrahim, M. Berrebia, A. Hamou, H. Kherief, Y. Zanoun, and K. Zenata, "Measure of carbon dioxide using a gas sensor of a semiconductor type based on tin dioxide (SnO 2)," *Journal of Materials and Environmental Science,* vol. 2, 01/01 2011.

[41] V. Rotar, "HEALTH STATE MONITORING SYSTEM DESIGN," MASTER OF SCIENCE, Electrical and Electronic Engineering, California State University, Sacramento, 2012.

[42] A. A. a. A. F. P. C. Bambang Dwi Kuncoro, "Smart Wireless CO2 Sensor Node for IoT Based Strategic Monitoring Tool of The Risk of The Indoor SARS-CoV-2 Airborne Transmission," *MDPI,* vol. 12, 2022.

[43] s. electronics. *MG-811 CO2 Sensor Module*. Available: https://sandboxelectronics.com/?p=147

[44] R. J. Asher, "Capnographic Analysis for Disease Classification," Master of Science, Electrical and Computer Engineering, , Carnegie Mellon University, 2012.

[45] S. Ramanathan, M. B. Malarvili, and S. C. B. Gopinath, "Assessing respiratory complications by carbon dioxide sensing platforms: Advancements in infrared radiation technology and IoT integration," *Arabian Journal of Chemistry,* vol. 16, no. 2, p. 104478, 2023/02/01/ 2023.

[46] K. Nonami *et al.*, "DEVELOPMENT OF MINE DETECTION ROBOT COMET-II AND COMET-III," *The Proceedings of the International Conference on Motion and Vibration Control,* vol. 6.1, pp. 449-454, 01/01 2002.

[47] plot.ly. (2023). *Sensor data from The CYD climate sensor*. Available: https://rawgit.com/Rovanion/comet-sensor/master/examples/2016-04-25%20-%202016-04-30.html

[48] O. P. Singh, T. A. Howe, and M. B. Malarvili, "Real-time human respiration carbon dioxide measurement device for cardiorespiratory assessment," *Journal of Breath Research,* vol. 12, no. 2, p. 026003, 2018/01/03 2018.

[49] E. B. Mary Kay Bates, Molly Love Parrucci, and Douglas Wernerspach, "Evaluating Infrared Carbon Dioxide Sensors for 21st Century Cell Culture: Introducing the Thermo Scientific IR180Si Infrared CO2 sensor," *Thermo Fisher Scientific Inc,* 2014.

[50] L. Mendes, N. Ogink, N. Edouard, H. J. Dooren, I. Tinôco, and J. Mosquera, "NDIR Gas Sensor for Spatial Monitoring of Carbon Dioxide Concentrations in Naturally Ventilated Livestock Buildings," *Sensors,* vol. 15, pp. 11239-11257, 05/13 2015.

[51] H. Rehouma, R. Noumeir, S. Essouri, and P. Jouvet, "Advancements in Methods and Camera-Based Sensors for the Quantification of Respiration," (in eng), *Sensors (Basel),* vol. 20, no. 24, Dec 17 2020.

[52] Masimo. (2023). *Capnography and Gas Monitoring Solutions*. Available: https://www.masimo.com/technology/ventilation-and-respiration/capnography/

Auns Q. H. Al-Neami has done her bachelor's degree from Electrical engineering college / University of technology in 1996. She has done her master's degree from Electrical engineering college / University of technology in 1999.She has completed her PhD degree in Biomedical Signal processing and analysis from Electrical engineering college / University of technology in 2004.

She had about 40 researches and 20 conference participations, teaching measurement system, AI and expert system, Electric and electronic circuits and in Al-Nahrain University in Biomedical engineering department.

Zina Ali Abed has done her bachelor's degree from Al-Nahrain University/ College of Engineering in 2012. She has done her master's degree in Biomedical Engineering from Al-Nahrain University/ College of Engineering in 2022.